An adder behavior in mammalian cells achieves size control by modulation of growth rate and cell cycle duration

Authors:

Clotilde Cadart[1,2], Sylvain Monnier[1,3], Jacopo Grilli[4], Rafaele Attia[1,2], Emmanuel Terriac[1,5], Buzz Baum[6,7], Marco Cosentino-Lagomarsino[8,9,10,§], Matthieu Piel[1,2§]

Affiliations :

[1] Institut Curie, PSL Research University, CNRS, UMR 144, F-75005, Paris, France

[2] Institut Pierre-Gilles de Gennes, PSL Research University, F-75005, Paris, France

[3] Univ. Lyon, Université Claude Bernard Lyon 1, CNRS, Institut Lumière Matière, F-69622, Villeurbanne, France

[4] Department of Ecology and Evolution, University of Chicago, 1101 E 57th Street, Chicago, Illinois 60637, USA

[5] Current address: INM-Leibniz Institute for New Materials, Campus D2 2, 66123 Saarbrücken, German

[6] MRC Laboratory for Molecular Cell Biology, UCL, London, United Kingdom

[7] Institute of Physics of Living Systems, UCL, London, United Kingdom

[8] Sorbonne Universités, Université Pierre et Marie Curie, Paris, France

[9] CNRS, UMR 7238 Computational and Quantitative Biology, Paris, France

[10] FIRC Institute of Molecular Oncology (IFOM), Milan, Italy

§ Correspondence should be sent to: marco.cosentino-lagomarsino@upmc.fr and matthieu.piel@curie.fr (**lead contact**)

Summary

Despite decades of research, it remains unclear how mammalian cell growth varies with cell size and across the cell division cycle to maintain size control. Answers to this question have been limited by the difficulty of directly measuring growth at the single cell level. Here, using a variety of cultured mammalian cell lines, we report direct measurement of single cell volumes over a complete cell division cycle. We show that the volume added across the cell cycle is independent of cell birth size, a size homeostasis behavior called “adder”. We propose a mathematical framework that can be used to characterize the full spectrum of size homeostasis mechanisms from bacteria to mammalian cells. This reveals that a near-adder is the most common type of size regulation, but shows that it can arise from various types of coupling between cell size, cell growth rate and cell cycle progression.

Keywords

Cell volume, cell size homeostasis, cell division cycle, mammalian cells, growth rate, microchannels, microfabrication, live cell microscopy

Introduction

Most proliferating cells are able to grow and divide in such a way as to maintain their size within a well-defined range under defined environmental conditions. Understanding how this is achieved has been a long-standing question in biology. Recently, however, spectacular progress has been made to understand how a variety of unicellular organisms control their size and shape as they pass through the cell cycle (Sauls, Li, and Jun 2016) thanks to live cell imaging, the development of microfluidics platforms that can maintain cell number and nutrient conditions, together with quantitative image analysis (Wang et al. 2010; Lyer-Biswas et al. 2014). This work has helped to define a small number of simple rules for cell size homeostasis in yeast and bacteria (Sauls, Li, and Jun 2016). However, similar progress has yet to be made for animal cells, which have a flexible cell shape that complicates the analysis.

As a result, most studies in the field thus far have relied on population level measures to assess mammalian cell growth control (Ian Conlon and Raff 2003; Dolznig et al. 2004; Echave, Conlon, and Lloyd 2007; Killander and Zetterberg 1965; R. Kafri et al. 2013). These include attempts to extrapolate growth dynamics from size measurements at fixed time-points across a population (R. Kafri et al. 2013; Sung et al. 2013; Tzur et al. 2009). Recently researchers have returned to the question using a variety of parameters as proxies for size at the single cell level. These include cell mass (Park et al. 2010; Sung et al. 2013; Mir et al. 2011), buoyant cell mass (Son et al. 2012a) and density (Grover et al. 2011). While most of these measurements have been indirect (Popescu et al. 2014), some studies have reported single live cell measurement of mass (Mir et al. 2014; Park et al. 2010) or buoyant mass (Son et al. 2012a) over complete cell cycles.

Given the difficulties of accurately measuring mammalian cell size over multiple cell cycles, most of these studies have focused their attention on the pattern of growth, with the assumption that growth control only need be important for cells that have an exponential pattern of growth, i.e. for cells that grow faster when they are bigger (as they might do if ribosome density remained constant with cell size). This focus on growth dynamics has further complicated matters, since some studies have suggested that growth is linear in some mammalian cells (Ian Conlon and Raff 2003), while time modulation in G1 has been hypothesized in earlier work (Dolznig et al. 2004; Killander and Zetterberg 1965). Other researchers have concluded using other cell types that growth, although exponential on average, is modulated at specific points across the cell cycle and that changes in growth rate contribute to cell size control (Tzur et al. 2009; R. Kafri et al. 2013). Direct evidence supporting this hypothesis was provided for lymphoblastoid cells, which display no significant cell cycle time modulation but for which a convergence of growth speeds was observed at G1/S transition (Son et al. 2012a).

There is an additional problem in the study of size control in metazoan cells. These cells indeed evolved to respond to growth and proliferation signals (e.g. growth factors or mitogens) determined at the tissue, organ or organismal level during development, regeneration or homeostasis at the adult stage (Edgar 2006; Saucedo and Edgar 2002). This has led some authors to doubt the existence of intrinsic regulatory mechanisms that might work together with extrinsic signals to coordinate growth and cell cycle progression at the single cell level (Lloyd 2013; Edgar 2006). Conversely, others have provided evidence of size or growth-dependent progression through G1 in cultured cells (Killander and Zetterberg 1965; Dolznig et al. 2004) and in the developing fly (Edgar 2006), reminiscent of what has been observed in budding yeast (Johnston 1977; Hartwell and Unger 1977). In summary, it remains

hotly debated whether or not animals cells possess active mechanisms of cell size control and, if so, how they may operate.

While there is no consensus about the way animal cells control their size, the work in single celled yeast and bacteria has led to the development of a better understanding of mechanisms by which cells can control their size. In general then, size homeostasis is achieved by cells adapting the amount of growth across their entire cell division cycle to their initial size, i.e. large cells should grow less, while small cells should grow more. These homeostatic behaviors are usually grouped into three main categories: the sizer, the adder and the timer. The classical example of a sizer is the behavior of the fission yeast, *S. Pombe* (Fantes 1977), where a size threshold was proposed to control the passage of cells across several key cell cycle transitions. By contrast, the adder mechanism relies on the addition of a constant amount of growth at each cell cycle that is independent of initial size (Amir 2014; Voorn and Koppes 1998), causing cells to converge on an average size, equal to the mean added volume, independently of their starting size. This behavior has been observed in several datasets for bacteria and in budding yeast (Campos et al. 2014; Taheri-Araghi et al. 2015; Soifer et al. 2016). This adder-type behavior can be achieved by combining linear growth with a constant cell cycle time (a process called 'timer') (Ian Conlon and Raff 2003). But in most cells and conditions studied, growth has been reported to be exponential - causing timer mechanisms to fail as bigger cells grow more than small cells in the same period. Importantly, while the phenomenological description of the size homeostatic process as a sizer, adder or timer defines the rate of size convergence in a population of proliferating cells, several distinct molecular mechanisms can achieve the same global behavior. Moreover, these simple categories are only extreme cases of correlations between size, duration of the cycle, and growth. Thus, entry time into the next stage may depend on both size and time ('concerted control' (Osella, Nugent, and Cosentino Lagomarsino 2014)), or an "imperfect" adder or sizer may be in place (Jun and Taheri-Araghi 2015), and size corrections may correspond to statistical biases rather than clear deterministic effects (Osella, Tans, and Cosentino Lagomarsino 2017). Additionally, different cell-cycle sub-periods may be subject to different controls (Adiciptaningrum et al. 2015; Wallden et al. 2016; Delarue, Weissman, and Hallatschek 2016), so that the overall emergent pattern could become complex. These factors make it all the more remarkable that simple patterns, like a near adder, have ever been observed.

While the recent body of literature on cultured mammalian cells homeostasis raised several important questions, it remains difficult to compare with what is known on bacteria and yeasts. For example, as yet there is no data to test how final volume (at mitosis onset) relates to initial volume (at birth) for individual cultured mammalian cycling cells. As a consequence, despite decades of work and discussion, it is not known if mammalian cells behave more like adders, sizers or timers. Moreover, it is not known if this is likely to vary across cell types.

To address this question we recently developed two new methods that allow us to precisely measure the volume of single live cells over several days, on a large number of cells, independently of their shape (Clotilde Cadart et al. 2017; Zlotek-Zlotkiewicz et al. 2015; C. Cadart et al. 2014). In this study, we used these tools to measure the size of various mammalian cell lines for up to 50 hours, over two complete cell cycles. Our analysis reveals that most cells use an adder type mechanism to maintain their size across cycles, which is achieved thanks to a modulation of G1 duration according to initial cell size. Building on this we have developed a general framework by which to compare cell size control across all the systems thus far studied.

Results

Single cell volume measurement over complete cell division cycles

Cultured mammalian cells display a broad range of sizes (Ginzberg, Kafri, and Kirschner 2015) (Figure S1A), which is due in part to the various cell cycle stages present in a population of cycling cells, and in part to the distribution of their size at birth. It is a general belief that proliferating cultured cells double their size between two divisions, yet the relation, for single cells, between their size at mitotic entry and their size at birth, has never been reported for cultured mammalian cells.

To establish this relation, it is necessary to track single proliferating cells and measure the volume of the same cell at birth and at mitotic entry. We implemented two distinct methods to obtain these measures. First, we grew cells inside microchannels of a well-defined cross-sectional area (Figure S1B, and (Cadart et al. 2014)). In such a geometry, dividing cells occupied the whole section of the channels and we could infer their volume from their length, like for yeasts and bacteria. The second method we used was based on fluorescence exclusion (FXm, (Zlotek-Zlotkiewicz et al. 2015; Cadart et al. 2017), Figure 1A, Movie S1) and has been optimized for long term recording and automated analysis of populations of growing cells ((Cadart et al. 2017), Figure S1C and supplementary information). It is more precise than the channels method and also produces complete growth trajectories for single cells (Figure 1B-C and S1D). Visual inspection of the movies was used to determine key points in the cell division cycle for each single cell tracked. Volume at birth was defined as the volume of a daughter cell 40 minutes after cytokinesis onset, while volume at mitotic entry was defined as volume of the same cell 60 minutes prior to the next cytokinesis onset (Figure 1B). These intervals were chosen to avoid the period of volume overshoot corresponding to mitosis (Zlotek-Zlotkiewicz et al. 2015; Son et al. 2015) (Figure S1E). We verified that the sum of the volumes of the two daughter cells at birth corresponded to the volume of the mother cell prior to mitotic entry, when birth and mitotic entry volumes were determined this way (Figure S1E-F). Single growth trajectories were also examined (Figure S1D), and analysis of growth speed as a function of size, for a large number of single cells and cell aggregates showed global exponential growth, as expected (Figure S1G) (Tzur et al. 2009; Mir et al. 2011; Sung et al. 2013; Son et al. 2012a). For each experiment performed, the dataset was checked for quality: we verified that the distribution of volumes at birth and the average growth speed did not change throughout the experiment, and that these values did not change from one experiment to another (Figures 1D and S1H). All the experiments in our dataset match these quality criteria (note that we kept one dataset which showed a significant, but small, decrease in volume through the course of the experiment, because despite optimization, we could not avoid some internalization of dextran by these cells, Figure S1H HeLa cells). We were thus able, with these methods, to produce fully validated high quality datasets of single cell volume along cycles of growth and division, which can be further used to ask elementary questions on volume homeostasis for proliferating cultured mammalian cells.

The adder behavior is common in cultured mammalian cells

The first elementary information comes from the relation between the added volume and the volume at birth. We thus made that plot, together with the equivalent plot of volume at mitotic onset versus volume at birth, for each cell line and condition in our dataset (Figure 2A and S2A). If cells were doubling their volume, the added volume would be equal to the volume at birth, thus the two values would linearly correlate with a slope of 1, and the final versus initial volume plot would show a slope

of 2. On the other hand, if cells were perfectly correcting for differences in size, added volume would be smaller for bigger cells, so the slope would be negative, while the final volume would be identical for all cells independently of their initial volume. We studied 4 different cancerous cell lines (HT29, HeLa, MDCK and Raji) and found neither of these two extremes. With the exception of Raji cells (human B lymphoblast), which showed a large dispersion of added volumes, and for which added volume slightly correlated with initial volume (Figure S2A), we instead found that added volume showed no correlation with initial volume (Figure 2A, left panel). Consistently, the volume at mitotic entry showed a clear linear correlation with volume at birth, with a slope close to 1 (Figure 2A, right, and Figures 2B and S2A), suggesting that all cell lines studied, except the Raji cells, grew by the same amount, on average, independently of their volume at birth. This observation was also reproduced when analyzing previously published results obtained on lymphoblastoid L1210 cells kindly shared by the authors (Son et al. 2012). This behavior is known as an adder, and was already described for several bacterial species and for the buds of budding yeast cells (Campos et al. 2014; Taheri-Araghi et al. 2015; Soifer et al. 2016). This weak form of volume homeostasis was shown, theoretically and experimentally for bacteria and yeasts, to be able to compensate for asymmetries in sizes during division. A direct prediction is that, after an asymmetric division, the difference in size of the two daughter cells would be reduced by half in one division cycle, but not completely compensated. We artificially induced asymmetric divisions by growing cells inside microchannels (Figure S1B, Movie S2). Confinement prevents mitotic rounding, which leads to errors in the mitotic spindle positioning and ultimately generates uneven division of the mother cell (Figures 2C and S2B, (Lancaster et al. 2013; Cadart et al. 2014)). We then compared the asymmetry in volume, at birth and at the next mitosis, between pairs of daughter cells that had divided inside these channels. We found that their level of volume asymmetry at birth was much higher than in control cells that divided outside of the channels, and that it was significantly reduced at entry into the next mitosis, but not completely compensated (Figure 2D), as predicted with an adder behavior. In conclusion, this first analysis of our dataset revealed that most cultured mammalian cell lines display a typical adder behavior.

G1 duration is negatively correlated with volume at birth

When cells are growing exponentially, smaller cells grow less, in the same amount of time, than large cells. A simple way for small cells to add as much volume as big cells, is to grow for a longer time. This modulation of cell cycle duration, which is well established for the budding yeast (Hartwell and Unger 1977; Johnston 1977) was also proposed in the past for mammalian cells (Killander and Zetterberg 1965; Dolznig et al. 2004) but was not verified in more recent contributions (R. Kafri et al. 2013; Son et al. 2012a) opening a controversy on this question, with few direct observation available to clarify this point. In our dataset, cells grown in the volume measurement chamber, but not inside micro-channels, showed a longer cell division cycle for smaller cells (Figure S2A, middle graphs). To investigate this point in more details, we combined cell volume measurements on HT29 cells with a classical marker of cell cycle phases, hgeminin-mcherry, which accumulates in the cell nucleus at S-phase entry (Sakaue-Sawano et al. 2008) (Figures 3A, S3A and Movie S3). This new dataset confirmed that, at the scale of the entire cell division cycle, cells added the same amount of volume independently of their volume at birth. During G1 phase, small cells at birth added slightly more volume than large ones, while during S-G2, large cells at G1/S added slightly more volume than small ones (Figure 3B and S3B, left graphs). Consistently, the volume at G1/S transition plotted against volume at birth showed a slope below 1 ($a = 0.7 \pm 0.01$), suggesting a homeostasis mechanism more efficient than an adder, while the slope

of the volume at mitosis entry versus volume at the G1/S transition was 1.4 ± 0.02, suggesting a poor homeostasis mechanism (Figure S3B, right graphs). Consistent with a regulation occurring mostly in G1, the distribution of G1 durations was wide and right-skewed, resembling the distribution of entire cell division cycle durations (Figures 3C and S3C, CV=53%), while S-G2 showed a very narrow and symmetrical distribution of durations (Figures 3C and S3C, CV=18%) (Fligner-Kileen test comparing the standard deviations, p=2*10^-16). Consistently, the duration of G1 was highly correlated with the total duration of the cell cycle, while it was less for S-G2 (Figure S3D). Plotting the time spent for single cells in a given phase versus its volume at the beginning of that phase, confirmed that smaller cells at birth had a longer G1 phase, while smaller cells at the G1/S transition spent as much time as bigger cells in S-G2 (Figures 3D and S3B, middle graphs). This graph also suggested that there was a minimal time cells spent in G1, and that dispersion of G1 duration was larger for smaller than for larger cells, which tended to spend only a minimal time in G1 (about 4 to 5 hours). This is well illustrated by the cumulative distribution function of the time spent in G1 for various ranges of volumes at birth (Figure 3E). We could not distinguish between the effective adder observed from birth to mitosis and the alternative model currently debated in yeast (Soifer et al. 2016) and bacteria (Ho and Amir 2015) where the constant volume is added between two replication events (see supplementary information, Figures S3E-G). These data together suggest that, despite an overall exponential growth, smaller cells can add, on average, as much volume as bigger cells, thus achieving an adder behavior, by extending the duration of the G1 phase, while S-G2 phase rather resembles a timer, with a duration independent of size at the G1/S transition.

Abnormal large cells display a minimal G1 duration and a modulation of growth rate

Figures 3D-E show a lower limit on the duration of G1 phase, which implies that, if growth was exponential and homeostasis limited to the G1 phase, it would not be possible to have homeostasis for larger cells. To produce larger cells at birth, we arrested cells using Roscovitine, an inhibitor of major interphase cyclin dependent kinases, like Cdk2 (Meijer and Raymond 2003). For this experiment, we used HeLa cells, because HT29 cells, despite long arrest with Roscovitine treatment, only slightly increased their volume. After a 48hours block with Roscovitine, the drug was rinsed, and cells were injected in the volume measurement chamber. Recording started after the first mitosis following the release from Roscovitine. As expected, cells which had been treated with Roscovitine were on average 1.7 fold larger than the controls (Figure 4A and 4B, top histogram of the graph, Figure S4A). Single cell growth curves showed that Roscovitine treated cells behaved similarly to large control cells (Figure 4A, Movie S4). As expected, their G1 duration was shorter (Figure 4B right axis) and was on average closer to a minimal G1 duration (≈ 4 hours) independently of volume at birth (Figure 4B). Interestingly, this duration was the same as the duration displayed by large control cells. But, surprisingly, large Roscovitine treated cells still grew, during G1, by nearly the same amount of volume than smaller control cells, independently of volume at birth (Figure 4C). In S-G2 however, the duration was longer for Roscovitine-treated cells, maybe due to replication defects, and the added volume was thus also larger (Figure S4B-C). If G1 duration is not modulated and larger cells grow by the same amount, an alternative mechanism is that growth speed is modulated. We thus analyzed single cells growth curves in G1 and plotted their growth speed against their volume. It showed that, both for control cells and Roscovitin treated cells, and for all the range of sizes, growth speed increased with size, compatible with an exponential growth even for the largest cells (Figure 4D for G1, S4D-E for S-G2 and complete cell cycle, and S4F relative to G1/S transition). To understand how larger cells at birth could grow by

approximately the same amount as smaller cells, in a similar amount of time, and because single growth curve trajectories showed complex behaviors (Figure S4G-I), we binned cells by their size at birth and plotted, for small, intermediate and large cells at birth, their growth speed versus their volume. This showed that although, for all ranges of size at birth, growth was compatible with exponential, the slope of growth speed versus volume decreased for larger sizes at birth, suggesting a lower exponential growth rate for cells born bigger (Figure 4E). In conclusion, consistent with a minimal G1 duration, Roscovitine treated cells, which were as big or larger at birth than large control cells, displayed a G1 duration independent of their volume at birth and on average equal to the minimal G1 duration found for control cells. They still added the same amount of volume as smaller cells, due to a modulation of their exponential growth rate, with larger cells at birth showing a smaller growth rate. By producing larger cells at birth, we were able to observe the robustness of the adder behavior: despite a minimal G1 duration, larger cells still displayed an adder behavior concurrently with a modulation of their exponential growth rate as a function of their size at birth.

A general mathematical framework to compare the homeostatic process from bacteria to eukaryotes

This result prompted us to perform a comparative analysis on our whole dataset, and on other published datasets (Kennard et al. 2016; Taheri-Araghi et al. 2015; Kiviet et al. 2014; Soifer, Robert, and Amir 2016; Nobs and Maerkl 2014; Wallden et al. 2016), to ask how general was the adder behavior and how general were cell cycle timing or growth rate modulation. In order to be able to perform this comparison, it was necessary to define a simplified mathematical framework (described in supplementary information) applicable to the whole cell cycle or to single cell-cycle stages (for the sake of simplicity, we will discuss it hereon for an entire cycle). Our model assumes that cells grow exponentially, which corresponds to the most common behavior we observed in our dataset, and adopt a rate chosen stochastically from a probability distribution. This rate may depend on volume at birth (and hence contribute to size correction). Similarly, the interdivision time may be chosen based on volume at birth and has a stochastic component. Correlations between growth rate, interdivision time and size at birth are accounted to linear order, motivated by the fact that such linear correlations are able to explain most patterns in existing data (at least for bacteria, (Grilli et al. 2017)). The resulting model is able to characterize the joint correction of size by timing and growth rate modulation, with a small number of parameters.

A first parameter, λ, describes how the total relative growth depends on volume at birth. If $\lambda = 1$, the system behaves like a sizer, if it is 0.5, it is an adder and if it is 0, all cells double their initial volume and there is no size control at all. This parameter can be described, for each dataset, by performing a linear regression on the plot of $\log(V_{mitosis}/V_{birth})$ versus $\log(V_{birth})$ (Figures 5A, S5A and equation 5 in supplementary informations). The second parameter, θ, describes how interdivision time depends on volume at birth. This parameter can be described, for each dataset, by performing a linear regression on the plot of cell cycle duration ($\tau = \Delta T$) versus $\log(V_{birth})$ (Figures 5B, S5B and equation 6 in supplementary informations). If this correlation is negative (which, by choice, corresponds to a positive value of the parameter meant to describe the strength of the correction), it means that larger cells will tend to divide in shorter times, hence these cells operate size correction due to a modulation of timing. Finally, the third parameter, γ, describes the link between initial size and a variation in growth rate with respect to its mean value. This can be obtained by linear regression when the corresponding measurements are available (e.g. in data from bacteria, (Wallden et al. 2016; Kennard et al. 2016; Kiviet

et al. 2014; Taheri-Araghi et al. 2015) Figures 5C and S5C, equation 4 in supplementary information). When growth rate for single-cells was not available (for mammalian cells and yeasts), the parameter γ was estimated from the values of λ and θ using an approach based on the covariance between pairs of measured variables (Figure S5D-E and supplementary information). The validity of this approach was tested on the bacteria datasets where all parameters can be directly measured (Figure S5E and supplementary information).

These three parameters are linked by a balance relation, which describes the fact that the overall size correction results from the combination of timing and growth rate corrections (see also supplementary information).

$$\lambda = \theta \langle\alpha\rangle \langle\tau\rangle + \gamma \langle\alpha\rangle \langle\tau\rangle \quad \text{(Eq.1)}$$

Additional (less relevant here) parameters concern the intrinsic stochasticity of interdivision timing, growth rates and net growth (see supplementary information). For eukaryotes where the growth rate $\langle\alpha\rangle$ is not easily accessible, the product $\langle\alpha\rangle \langle\tau\rangle$ was approximated by $\langle G\rangle = \langle \log(V_{mitosis})/\log(V_{birth})\rangle$ (Figure 5D, right, supplementary information). The validity of this normalization was tested with bacteria (Figure S5F and supplementary information).

Using these dimensionless parameters, it was then possible to compare datasets obtained from different cell types in different conditions and estimate whether they displayed volume homeostasis ($\lambda > 0$) with an adder behavior ($\lambda = 0.5$) or better ($\lambda = 1$). It was also possible to know if homeostasis relied more on time modulation ($\theta > 0$) or growth rate modulation ($\gamma > 0$). For bacteria, which have clearly identifiable exponential growth for single cells, all three parameters can be evaluated directly (Figure 5D, left). With this framework (Figures 5E and S5G), all the datasets for both bacteria (Kennard et al. 2016; Wallden et al. 2016; Kiviet et al. 2014; Taheri-Araghi et al. 2015) and yeasts (Nobs and Maerkl 2014; Soifer, Robert, and Amir 2016) mostly fell around the line of $\lambda = 0.5$ indicative of a near-adder behavior (note that, as expected, the yeast *S. Pombe* showed a better than adder behavior, but not a perfect sizer, because larger cells still have a minimal growth period). These cells all showed a consistent degree of correction via time modulation ($\theta > 0$). A small subset also showed positive growth rate modulation ($\gamma > 0, \text{Figure 5E green side}$), but many also had instead a strong negative growth rate modulation (i.e. growth rate modulations contributed to noise in size instead of correcting it, Figure 5E blue side).

The adder behavior emerges from a variety of couplings between growth and time modulations

Each cell line and condition was characterized by one value for each parameter and thus one point on the graph which shows γ versus θ (Figure 5F). Most cells displayed volume homeostasis close to an adder behavior (all points fell clustered around the line representing $\lambda = 0.5$, Figure 5F), consistent with the plot shown in Figure 2B. Data obtained from Son et al (Son et al. 2012a) on L1210 showed that these cells were also adders, with mostly growth rate modulation (in accordance with the results of that study), but also some level of time modulation, possibly explained by the negative correlation between G1 duration and early growth speed observed in these cells (Son et al. 2012a) (Figure 5F, yellow star). For both mammalian cells and bacteria, no dataset showed a negative time modulation (bigger cells at birth having a longer cell division cycle, meaning that time modulation always contribute to homeostasis, although to a lesser extent in mammalian cells than in yeasts and bacteria.

Negative growth rate modulation (larger cells with a faster exponential growth rate than smaller cells at birth) was rarer in mammalian cells than in bacteria, but nevertheless observed in some cases (for Raji cells, Figure 5F, pink circle). This means that in mammalian cells, contrary to yeasts and bacteria, growth rate modulation always contributes to homeostasis and does it to a larger extent. Our analysis method, by providing a summarized overview of a large dataset comprising various cell types and culture conditions, demonstrated the robustness of the adder behavior, and also revealed the diversity of underlying homeostatic mechanisms, relying more on growth rate modulation or cell cycle duration modulation, even for a given cell line.

Discussion

Size homeostasis in cultured mammalian cells can be described phenomenologically as an adder behavior

Cell size homeostasis, or how cells regulate their size through cycles of growth and division, is one of the central questions of cell biology. Due to technical limitations, our understanding of this process in mammalian cells derives in large part from indirect evidence (Conlon et al. 2001; Ian Conlon and Raff 2003; Echave, Conlon, and Lloyd 2007; Tzur et al. 2009; Sung et al. 2013; R. Kafri et al. 2013; Dolznig et al. 2004), nurturing controversies which have proven hard to resolve. To make progress in this area, we have developed two new methods, microchannels and fluorescence exclusion, to follow the volume of single cultured mammalian cells over long periods of time. These data reveal that four out of five different cell lines tested, act as adders, meaning that the added volume across a cell cycle was independent of the volume at birth (Campos et al. 2014; Taheri-Araghi et al. 2015; Soifer, Robert, and Amir 2016). Our analysis also reveals the complexities behind this apparently simple phenomenological description of the process of cell size control.

Generality of the adder mechanism

In recent years, the adder mechanism has been observed in a variety of organisms, from bacteria (Soifer et al. 2016; Campos et al. 2014; Taheri-Araghi et al. 2015; Deforet et al. 2015) to yeast (Soifer et al. 2016). However, apparent universality of this simple result is deceiving. For example, theoretical work has shown that more data is required to support this conclusion (Grilli et al. 2017). Thus, experimental perturbations are required to test the systems robustness before one can conclude that an adder is in place. Here, by developing a method to induce asymmetric divisions, we were able to show that the size asymmetry was only reduced by half across one division cycle (Figure 2D) (Sauls, Li, and Jun 2016) – a key characteristic of the adder we identified through our analysis of unperturbed cell cycles.

Additionally, the use of the term adder has evolved from a simple phenomenological description of a behavior common to several organisms (Sauls, Li, and Jun 2016), to a more complex picture. The same organism can display a range of effective homeostatic behaviors depending on its growth rate both at the population level (Wallden et al. 2016) and at the individual cell level (Kennard et al. 2016).

Modulation of G1 duration

How is this adder achieved? Schematically, this could occur in two ways, i) via a change in growth rate or ii) via a change in cell cycle time. Moreover, it is important to determine where in the cell cycle it operates, and how it is affected by cell size – a pure adder mechanism could also potentially measure added size to trigger cell cycle progression independently of size or timing. This led us to test the role of cell division cycle timing modulation on the cell size control mechanism. For budding yeast, control is known to occur at G1/S, while for fission yeast, it is mostly occurring at G2/M (Turner, Ewald, and Skotheim 2012)

A role for the timing of G1/S transition in cell size control has long been hypothesized in mammalian cells as well (Zetterberg and Killander 1965; Dolznig et al. 2004), but a direct measurement that would allow a correlation between G1 duration and initial size has never been previously reported. Instead,

it was suggested that there is a decrease in the variability of growth speed at the G1/S transition and a negative correlation between early growth speed in G1 and G1 duration (Son et al. 2012). Here, we observed that the clear negative correlation between total cell cycle length and size at birth (Figures S2A central graphs), was mostly due to a negative correlation between G1 duration and volume at birth, for both HT29 and HeLa cells (Figures 3D-E, S3B-D and 4B) - reinforcing the notion that G1 progression and size are coupled. Moreover, in HT29 cells progression through G1 depended on both volume and time (Figure 3E) - suggesting that volume is not the sole variable limiting cell cycle progression.

Given the similarities both at the phenomenological and molecular level between *S. cerevisiae* and mammalian cells (Fisher 2016), it is possible to speculate that time modulation in G1 would depend on dilution of an inhibitor as was proposed for *S. cerevisiae* (Schmoller et al. 2015). A potential candidate for the minimal period could be the delay that was observed before inactivation of the APC-Cdh1 complex which has recently been proposed to set a minimal window of time of 4 hours before the commitment point to S phase in mammalian cells (Cappell et al. 2016).

A near timer in S/G2 and a minimal duration for G1

By contrast, S-G2 duration was less variable in duration and was poorly correlated with the total cycle time (Figures 3C and S3C-D). Moreover, there was no correlation between the length of S-G2 and volume at the G1/S transition in HT29 cells and control HeLa cells (Figures 3D, S3C-D and S4B), and cells with a shorter G1 did not have a longer S/G2 (Figures S5 G-I), suggesting that this phase had little impact on cell size homeostasis.

Both HeLa (Figure 4B) and HT29 cells (Figure 3D) display a minimum G1 duration of about 4-5 hours that is independent of cell volume. This is even clearer when HeLa cells are forced to divide at a large size, through treatment with Roscovitine (Figure 4B). A similar phenomenon was also reported before by Zetterberg and colleagues (Zetterberg and Killander 1965). Together with our study, these results suggest that G1 comprises two distinct periods: a first period, whose length might depend on cell size, possibly involving pRb-E2F activation (Cappell et al. 2016; Barr et al. 2016), and a second period with a constant duration of 4 hours ending with the inactivation of APC-Cdh1 (Cappell et al. 2016). This is strongly reminiscent of what was observed for yeast cells, breaking G1 up into a size-dependent pre-Start period and a timer-like post-Start period (Di Talia et al. 2007; Turner, Ewald, and Skotheim 2012; Schmoller et al. 2015).

Growth rate modulation at large cell sizes

The exponential character of growth is central to the question of cell size homeostasis (Mitchison 2003; Ginzberg et al. 2015). This led us to measure the growth speed of individual cells and for cell aggregates. Growth appeared exponential overall in all cases (growth speed increased as a function of cell size), even for the larger Roscovitine treated cells (Figures S1G, 4D and S4D-E). Consistently, when cells progressed through the cell cycle, and became on average bigger, their growth speed increased. Interestingly, when time was registered on the G1/S transition, it became clear that the growth speed increased less during S-G2 than in G1 (Figure S4F), although it is not clear whether this would contribute to size homeostasis. The picture was more complicated when investigating the growth of individual cells. Individual cells could display complex growth behaviors, alternating plateaus and

growth phases (Figures S5G-I), not clearly correlated with cell cycle stage events, even if plateaus were often seen in early G1. This suggests that growth in volume is on average exponential (when many cells are averaged, Figure S1D) but is, at the single cell level, modulated, maybe due to other factors that can fluctuate in time at the single cell level, like cell spreading area.

This result is in agreement with data in several recent studies that evaluated the growth of large cells under a condition of cell cycle arrest (Ian Conlon and Raff 2003; Tzur et al. 2009; R. Kafri et al. 2013), which suggested growth rates did not increase and/or declined with increasing cell size. Nevertheless, for cells born larger (like Roscovitine treated cells), which display on average a minimal G1 duration and thus loose the negative correlation between size at birth and G1 duration, it raises a concern: how can they still add, on average, the same volume as smaller cells at birth? Our data show that smaller cells at birth display a larger exponential growth rate than cells born larger (Figure 4E). Thus, depending on their initial size, cells appear to add volume at different rates as they grow. Similarly, in our experiments with HeLa and MDCK cells growing inside micro-channels, cells grew by the same amount in the same period of time, independently of their initial size (Figure S2A). In this setup, we were not able to follows single cells growth trajectories, but similarly to Roscovitin treated cells, they might operate in a regime of growth rate modulation rather than cell cycle time modulation. This could be due to the lateral confinement, limiting exchanges with the medium to the free ends of cells, which are defined by channel cross-sectional area and thus do not scale with volume (note that, since these experiments showed a constant average growth speed through time in the experiment, Figure S1H, we were confident that this was not due to a progressive depletion of nutrients). This more generally raises the question of how cells grow, and of the factors that can limit the exponential growth rate.

Limitations of protein synthesis (M. Kafri et al. 2016), nonlinear metabolic scaling with cell size (Miettinen and Björklund 2017) and physical constraints on volume growth via the addition of surface area (Glazier 2014) can all constrain cell growth. Whether any of them apply will depend on specific conditions. For example, the rate of protein synthesis slows down when mRNA supplies, which depend on the transcription from a finite number of DNA copies, become limiting in larger cells (Hu and Zhu 2014; M. Kafri et al. 2016). Mitochondrial activity and cell fitness are also maximum at a specific optimal size, after which they start decreasing (Miettinen and Bjorklund 2016). Finally, nutrient uptake, which depends on the cell surface area, can become limiting as the surface to volume ratio decreases in larger cells (Glazier 2014). Although all these factors could change the relation between growth speed and cell size, it is not clear how they would modulate the average growth rate as a function of size at birth. The mechanism that underlies this modulation of growth rate – a phenomenon essential for the robustness of the adder behavior – remains mysterious.

A simple general framework to summarize and compare homeostatic phenomenology in different datasets

To put these data into context, we developed a general framework by which to compare how growth rate and cell cycle time contribute to cell size control in different systems (Figure 5). In this way, it is possible to define three main types of coupling observed in our experiments and to compare them to data from other systems (and obtained by others).

First, when cultured in FXm chambers, epithelial HT29 and HeLa cells grow exponentially (Figures S1G, 4D, S4D-E). In this case, consistent with previous indirect findings on mammalian cells (Zetterberg and

Killander 1965; Dolznig et al. 2004), and reminiscent of the size control mechanism occurring in *S.cerevisiae* (Johnston 1977; Hartwell and Unger 1977; Di Talia et al. 2007), G1 duration is negatively correlated with cell volume at birth (Figures 3D and 4B).

Second, large HeLa cells reach a minimum duration of G1 (Figure 4B) and thus do not show modulation of G1 duration as a function of initial size. We also observed this behavior for cells grown inside confining channels, and it was reported in other articles, such as Son et al. (Son et al. 2012a), for which the authors kindly shared their original data with us. In all these cases an adder is still observed. For large HeLa cells, we could show that it is made possible by a modulation of the exponential growth rate as a function of size at birth (Figure 4E). Alternatively, growth rate could saturate for larger sizes, but we did not observe this phenomenon in our dataset.

Overall, our work reveals that there are at least three main aspects limiting cell growth and cell cycle progression: first, G1 progression is lengthened for small cells at birth, consistent with the hypothesis of a titration mechanism coupling growth and cell cycle timing (Schmoller et al. 2015; Soifer et al. 2016; Ho and Amir 2015). Second, there appears to be a minimum G1 passage time of close to 4-5 hours, consistent with recent findings on G1 regulation (Cappell et al. 2016; Zetterberg and Killander 1965). Third, exponential growth rate appears to also be modulated as a function of cell size at birth. Nevertheless, under all these conditions cells exhibit the same behavior – that of adders. How can this behavior arise? Although this seems remarkable, the same behavior under all these conditions could be driven by a single underlying mechanism, e.g. via molecular counting, when a fixed numbers of molecules must be synthesized or degraded in a way that does not depend on the growth rate before cells can undergo passage through G1 (Ho and Amir 2015). How this works remains to be determined, not just in mammalian cells but also in E. coli, where Harris and Theriot (Harris and Theriot 2016) hypothesized that the adder behavior might be a consequence of the rate-limiting step for division being due to septum completion, thus to a universal constraint in terms of surface growth. However, Wallden and colleagues recently showed that cells displayed stronger size homeostasis at low growth rates, getting close to a sizer (Wallden et al. 2016), complicating the matter. One might speculate that the type of adder described here may be a simple mode by which cells are able to grow as fast as possible without diverging in size. This could also explain the remarkable convergence between cells from different organisms that have very different growth mechanism, but share the fact that they have been maintained in rich culture conditions, with constant and unlimited growth factors and nutrients.

Size homeostasis in tissues

Our work suggests that mammalian cells possess intrinsic size regulation mechanisms with distinct limiting processes that contribute to size homeostasis, which we observed in cultured cells. Importantly, our observations are compatible with previous findings that had raised a doubt about the existence of size control in mammalian cells such as the fact that growth speed modulation rather than time modulation account for size control (Conlon and Raff2003), or that at very fast growth, the duration of the cell cycle reaches an intrinsic minimal duration (Edgar 2006). These behaviors could also exist within tissues and constitute the cell intrinsic basis on which tissue scale signals act to regulate cell size. A recent study on brain development in drosophila showed that a modification of cell metabolism during metamorphosis makes some nutrients limiting, leading to a gradual reduction of neuronal progenitors size, as they do not grow enough during each cycle and eventually reach a minimal size at which they stop dividing (Homem et al. 2014). This might be due to a limit of the homeostatic mechanism, at very low growth rates, with an upper limit to cell division cycle duration,

and the existence of a minimal cell size to enter the cell division cycle. This study constitutes an incentive to explore further the phase diagram of growth behavior in single cultured cells, towards limits of slow growth rates and small cell sizes. As the description of single cell size homeostasis evolves towards that of a flexible process that involves several types of regulation of growth and cell cycle progression depending on the growth conditions, we envision the possibility of unifying the understanding of cell size regulation from single cell intrinsic mechanisms to tissues scale signaling.

Authors contributions

C.C. and S.M. conducted the experiments, S.M. optimized and designed the FXm chambers, E.T. and R.A. designed, produced and characterized the molds for the chambers, M.C-L. and J.G. developed the theoretical framework, B.B. helped conceive of project, helped supervise early part, helped with text, C.C. conducted the analysis, M.C-L. helped with data analysis, C.C. and M.C-L helped with the manuscript preparation, C.C. and M.P. designed the experiment, M.P. wrote the paper and supervised the work.

Acknowledgements

We would like to thank the Gerlich lab for sharing the HeLa-MP cell line, Helen K. Matthews, Nunu Mchedlichvili and Ewa Zlotek-Zlotkiewicz, members of the Piel lab and the Perez lab for scientific and technical advices, Camille Blakeley and Charlotte Pirot for preliminary works as undergrad students, Isabel Brito for advices on the statistical analysis, the imaging platform from the Institut Curie PICT-IBiSA, the UMR 168 clean room facility and the IPGG plateform. We also greatly acknowledge Jan Skotheim for critical reading of the manuscript and in depth comments on our work. CC acknowledges support from the Fondation pour la Recherche Médicale and the Ligue Nationale contre le Cancer for funding. MCL acknowledges support from the International Human Grantier Science Program Organization, grant RGY0070/2014. BB acknowledges Cancer Research UK programme grant for support: C1529/A17343. This work was supported by a LABEX IPGG grant to R.A., by an ERC consolidator grant (311205 PROMICO) to M.P., by an ANR grant to M.P. (ANR-14-CE11-0009-03, CellSize).

References

Adiciptaningrum, Aileen, Matteo Osella, M. Charl Moolman, Marco Cosentino Lagomarsino, Sander J. Tans, SJ. Tans, A. Amir, et al. 2015. “Stochasticity and Homeostasis in the E. Coli Replication and Division Cycle.” *Scientific Reports* 5 (December). eLife Sciences Publications Limited: 18261. doi:10.1038/srep18261.

Amir, Ariel. 2014. “Cell Size Regulation in Bacteria.” *Physical Review Letters* 112 (20): 208102. doi:10.1103/PhysRevLett.112.208102.

Barr, Alexis R., Frank S. Heldt, Tongli Zhang, Chris Bakal, and Béla Novák. 2016. “A Dynamical Framework for the All-or-None G1/S Transition.” *Cell Systems* 2 (1): 27–37. doi:10.1016/j.cels.2016.01.001.

Cadart, C., E. Zlotek-Zlotkiewicz, M. Le Berre, M. Piel, and H.K. Matthews. 2014. “Exploring the Function of Cell Shape and Size during Mitosis.” *Developmental Cell* 29 (2). doi:10.1016/j.devcel.2014.04.009.

Cadart, Clotilde, Ewa Zlotek-Zlotkiewicz, Larisa Venkova, Olivier Thouvenin, Victor Raacine, Maël Le Berre, Sylvain Monnier, and Matthieu Piel. 2017. “Fluorescence eXclusion Measurement of Volume in Live Cells.” *Methods in Cell Biology* 139 (Cell polarity and morphogenesis): 103–20. doi:10.1016/j.jwb.2007.10.005.

Campos, Manuel, Ivan V. Surovtsev, Setsu Kato, Ahmad Paintdakhi, Bruno Beltran, Sarah E. Ebmeier, and Christine Jacobs-Wagner. 2014. "A Constant Size Extension Drives Bacterial Cell Size Homeostasis." *Cell* 159 (6). Elsevier Inc.: 1433–46. doi:10.1016/j.cell.2014.11.022.

Cappell, Steven D, Mingyu Chung, Ariel Jaimovich, Sabrina L Spencer, and Tobias Meyer. 2016. "Irreversible APCCdh1 Inactivation Underlies the Point of No Return for Cell-Cycle Entry." *Cell* 166 (1). Elsevier Inc.: 167–80. doi:10.1016/j.cell.2016.05.077.

Conlon, Ian, and Martin Raff. 2003. "Differences in the Way a Mammalian Cell and Yeast Cells Coordinate Cell Growth and Cell-Cycle Progression." *Journal of Biology* 2 (1). BioMed Central: 7. doi:10.1186/1475-4924-2-7.

Conlon, Ij, Ga Dunn, Aw Mudge, and Mc Raff. 2001. "Extracellular Control of Cell Size." *Nature Cell Biology* 3 (October 2001): 3–7. http://discovery.ucl.ac.uk/186032/.

Deforet, Maxime, Dave Van Ditmarsch, and Joao Xavier. 2015. "Cell-Size Homeostasis and the Incremental Rule in a Bacterial Pathogen." *Biophysical Journal* 109 (3): 521–28. doi:10.1016/j.bpj.2015.07.002.

Delarue, Morgan, Daniel Weissman, and Oskar Hallatschek. 2016. "A Simple Molecular Mechanism Explains Multiple Patterns of Cell-Size Regulation." *bioRxiv* 1 (22): 2013–16.

Dolznig, Helmut, Florian Grebien, Thomas Sauer, Hartmut Beug, and Ernst W Müllner. 2004. "Evidence for a Size-Sensing Mechanism in Animal Cells." *Nature Cell Biology* 6 (9): 899–905. doi:10.1038/ncb1166.

Echave, Pedro, Ian J. Conlon, and Alison C. Lloyd. 2007. "Cell Size Regulation in Mammalian Cells." *Cell Cycle* 6 (2): 218–24. doi:10.4161/cc.6.2.3744.

Edgar, Bruce A. 2006. "How Flies Get Their Size: Genetics Meets Physiology." *Nature Reviews Genetics* 7 (12): 907–16. doi:10.1038/nrg1989.

Fantes, P A. 1977. "Control of Cell Size and Cycle Time in Schizosaccharomyces Pombe." *J Cell Sci* 24: 51–67. http://jcs.biologists.org/cgi/reprint/24/1/51.

Fisher, Robert P. 2016. "Getting to S: CDK Functions and Targets on the Path to Cell-Cycle Commitment." *F1000Research* 5: 2374. doi:10.12688/f1000research.9463.1.

Ginzberg, M. B., R. Kafri, and M. Kirschner. 2015. "On Being the Right (Cell) Size." *Science* 348 (6236): 1245075–1245075. doi:10.1126/science.1245075.

Glazier, Douglas. 2014. "Metabolic Scaling in Complex Living Systems." *Systems* 2 (4). Multidisciplinary Digital Publishing Institute: 451–540. doi:10.3390/systems2040451.

Grilli, Jacopo, Matteo Osella, Andrew S. Kennard, and Marco Cosentino Lagomarsino. 2017. "Relevant Parameters in Models of Cell Division Control." *Physical Review E - Statistical, Nonlinear, and Soft Matter Physics* 32411 (95). doi:10.1103/PHYSREVE.95.032411.

Grover, William H, Andrea K Bryan, Monica Diez-Silva, Subra Suresh, John M Higgins, and Scott R Manalis. 2011. "Measuring Single-Cell Density." *Proceedings of the National Academy of Sciences of the United States of America* 108 (27): 10992–96. doi:10.1073/pnas.1104651108.

Harris, Leigh K., and Julie A. Theriot. 2016. "Relative Rates of Surface and Volume Synthesis Set Bacterial Cell Size." *Cell* 165 (6). Elsevier Inc.: 1479–92. doi:10.1016/j.cell.2016.05.045.

Hartwell, LH, and MW Unger. 1977. "Unequal Division in the Control Division and Its Implications for the Control of Cell Division." *The Journal of Cell Biology* 75: 422–35.

Ho, Po-yi, and Ariel Amir. 2015. "Simultaneous Regulation of Cell Size and Chromosome Replication in Bacteria." *Frontiers in Microbiology* 6 (July): 1–10. doi:10.3389/fmicb.2015.00662.

Homem, Catarina C.F., Victoria Steinmann, Thomas R. Burkard, Alexander Jais, Harald Esterbauer, and Juergen A. Knoblich. 2014. "Ecdysone and Mediator Change Energy Metabolism to Terminate Proliferation in Drosophila Neural Stem Cells." *Cell* 158 (4). Elsevier Inc.: 874–88. doi:10.1016/j.cell.2014.06.024.

Hu, Yucheng, and Tianqi Zhu. 2014. "Cell Growth and Size Homeostasis in Silico." *Biophysical Journal* 106 (5): 991–97. doi:10.1016/j.bpj.2014.01.038.

Lyer-Biswas, S., C. S. Wright, J. T. Henry, K. Lo, S. Burov, Y. Lin, G. E. Crooks, S. Crosson, A. R. Dinner, and N. F. Scherer. 2014. "Scaling Laws Governing Stochastic Growth and Division of Single Bacterial Cells." *Proceedings of the National Academy of Sciences*, 1403232111-. doi:10.1073/pnas.1403232111.

Johnston, G. C. 1977. "Cell Size and Budding during Starvation of the Yeast Cell Size and Budding During Starvation of the Yeast." *Journal of Bacteriology* 132 (2): 738–40.

Jun, Suckjoon, and Sattar Taheri-Araghi. 2015. "Cell-Size Maintenance: Universal Strategy Revealed." *Trends in Microbiology* 23 (1). Elsevier Ltd: 4–6. doi:10.1016/j.tim.2014.12.001.

Kafri, Moshe, Eyal Metzl-Raz, Ghil Jona, Naama Barkai, A. Mayo, E. Dekel, U. Alon, et al. 2016. "The Cost of Protein Production." *Cell Reports* 14 (1). Elsevier: 22–31. doi:10.1016/j.celrep.2015.12.015.

Kafri, Moshe, Eyal Metzl-Raz, Felix Jonas, and Naama Barkai. 2016. "Rethinking Cell Growth Models." *FEMS Yeast Research* 16 (7): 1–13. doi:10.1093/femsyr/fow081.

Kafri, Ran, Jason Levy, Miriam B Ginzberg, Seungeun Oh, Galit Lahav, and Marc W Kirschner. 2013. "Dynamics Extracted from Fixed Cells Reveal Feedback Linking Cell Growth to Cell Cycle." *Nature* 494 (7438). Nature Publishing Group: 480–83. doi:10.1038/nature11897.

Kennard, Andrew S., Matteo Osella, Avelino Javer, Jacopo Grilli, Philippe Nghe, Sander J. Tans, Pietro Cicuta, and Marco Cosentino Lagomarsino. 2016. "Individuality and Universality in the Growth-Division Laws of Single E. Coli Cells." *Physical Review E - Statistical, Nonlinear, and Soft Matter Physics* 93 (1): 1–18. doi:10.1103/PhysRevE.93.012408.

Killander, D, and A Zetterberg. 1965. “Quantitative Cytochemical Studies on Interphase Growth II Derivation of Synthesis Curves from the Distribution of DNA, RNA and Mass Values of Individual Mouse Fibroblasts in Vitro.” *Experimental Cell Research* 39: 22–32.

Kiviet, Daniel J., Philippe Nghe, Noreen Walker, Sarah Boulineau, Vanda Sunderlikova, and Sander J. Tans. 2014. “Stochasticity of Metabolism and Growth at the Single-Cell Level.” *Nature* 514 (7522). Nature Publishing Group: 376–79. doi:10.1038/nature13582.

Lancaster, Oscar M, Maël Le Berre, Andrea Dimitracopoulos, Daria Bonazzi, Ewa Zlotek-Zlotkiewicz, Remigio Picone, Thomas Duke, Matthieu Piel, and Buzz Baum. 2013. “Mitotic Rounding Alters Cell Geometry to Ensure Efficient Bipolar Spindle Formation.” *Developmental Cell* 25 (3): 270–83. doi:10.1016/j.devcel.2013.03.014.

Lloyd, Alison C. 2013. “The Regulation of Cell Size.” *Cell* 154 (6). Elsevier Inc.: 1194–1205. doi:10.1016/j.cell.2013.08.053.

Meijer, Laurent, and Eric Raymond. 2003. “Roscovitine and Other Purines as Kinase Inhibitors . From Starfish Oocytes to Clinical Trials Roscovitine and Other Purines as Kinase Inhibitors . From Starfish Oocytes to Clinical Trials.” *Acc. Chem. Res* 36 (6): 417–25. doi:10.1021/ar0201198.

Miettinen, Teemu P., and Mikael Bjorklund. 2016. “Cellular Allometry of Mitochondrial Functionality Establishes the Optimal Cell Size.” *Developmental Cell* 39 (3): 370–82. doi:10.1016/j.devcel.2016.09.004.

Miettinen, Teemu P., and Mikael Björklund. 2017. “Mitochondrial Function and Cell Size: An Allometric Relationship.” *Trends in Cell Biology* xx. Elsevier Ltd: 1–10. doi:10.1016/j.tcb.2017.02.006.

Mir, Mustafa, Anna Bergamaschi, Benita S Katzenellenbogen, and Gabriel Popescu. 2014. “Highly Sensitive Quantitative Imaging for Monitoring Single Cancer Cell Growth Kinetics and Drug Response.” *PloS One* 9 (2): e89000. doi:10.1371/journal.pone.0089000.

Mir, Mustafa, Zhuo Wang, Zhen Shen, Michael Bednarz, Rashid Bashir, Ido Golding, Supriya G Prasanth, and Gabriel Popescu. 2011. “Optical Measurement of Cycle-Dependent Cell Growth.” *Proceedings of the National Academy of Sciences of the United States of America* 108 (32): 13124–29. doi:10.1073/pnas.1100506108.

Mitchison, J.M. 2003. “Growth During the Cell Cycle.” *International Review of Cytology* 226: 165–258. doi:10.1016/S0074-7696(03)01004-0.

Nobs, Jean-Bernard, and Sebastian J Maerkl. 2014. “Long-Term Single Cell Analysis of S. Pombe on a Microfluidic Microchemostat Array.” Edited by Michael Polymenis. *PloS One* 9 (4). Public Library of Science: e93466. doi:10.1371/journal.pone.0093466.

Osella, Matteo, Eileen Nugent, and Marco Cosentino Lagomarsino. 2014. “Concerted Control of Escherichia Coli Cell Division.” *Proceedings of the National Academy of Sciences of the United States of America* 111 (9): 3431–35. doi:10.1073/pnas.1313715111.

Osella, Matteo, Sander J. Tans, and Marco Cosentino Lagomarsino. 2017. "Step by Step, Cell by Cell: Quantification of the Bacterial Cell Cycle." *Trends in Microbiology* xx. Elsevier Ltd: 1–7. doi:10.1016/j.tim.2016.12.005.

Park, Kidong, Larry J Millet, Namjung Kim, Huan Li, Xiaozhong Jin, Gabriel Popescu, N R Aluru, K Jimmy Hsia, and Rashid Bashir. 2010. "Measurement of Adherent Cell Mass and Growth." *Proceedings of the National Academy of Sciences of the United States of America* 107 (48): 20691–96. doi:10.1073/pnas.1011365107.

Popescu, Gabriel, Kidong Park, Mustafa Mir, and Rashid Bashir. 2014. "New Technologies for Measuring Single Cell Mass." *Lab on a Chip* 14 (4): 646–52. doi:10.1039/c3lc51033f.

Sakaue-Sawano, Asako, Hiroshi Kurokawa, Toshifumi Morimura, Aki Hanyu, Hiroshi Hama, Hatsuki Osawa, Saori Kashiwagi, et al. 2008. "Visualizing Spatiotemporal Dynamics of Multicellular Cell-Cycle Progression." *Cell* 132 (3): 487–98. doi:10.1016/j.cell.2007.12.033.

Saucedo, Leslie J., and Bruce a. Edgar. 2002. "Why Size Matters: Altering Cell Size." *Current Opinion in Genetics and Development* 12 (5): 565–71. doi:10.1016/S0959-437X(02)00341-6.

Sauls, John T., Dongyang Li, and Suckjoon Jun. 2016. "Adder and a Coarse-Grained Approach to Cell Size Homeostasis in Bacteria." *Current Opinion in Cell Biology* 38. Elsevier Ltd: 38–44. doi:10.1016/j.ceb.2016.02.004.

Schmoller, K.M, J.J. Turner, M. Kõivomägi, and J.M. Skotheim. 2015. "Dilution of the Cell Cycle Inhibitor Whi5 Controls Budding Yeast Cell Size." *Nature* (in press). doi:10.1038/nature14908.

Soifer, Ilya, Lydia Robert, and Ariel Amir. 2016. "Single-Cell Analysis of Growth in Budding Yeast and Bacteria Reveals a Common Size Regulation Strategy." *Current Biology* 26 (3). Elsevier Ltd: 356–61. doi:10.1016/j.cub.2015.11.067.

Soifer, Ilya, Lydia Robert, Ariel Amir, Ilya Soifer, Lydia Robert, and Ariel Amir. 2016. "Single-Cell Analysis of Growth in Budding Yeast and Bacteria Reveals a Common Size Regulation Report Single-Cell Analysis of Growth in Budding Yeast and Bacteria Reveals a Common Size Regulation Strategy." *Current Biology* 26 (3): 356–61. doi:10.1016/j.cub.2015.11.067.

Son, Sungmin, Joon Ho Kang, Seungeun Oh, Marc W. Kirschner, T. J. Mitchison, and Scott Manalis. 2015. "Resonant Microchannel Volume and Mass Measurements Show That Suspended Cells Swell during Mitosis." *Journal of Cell Biology* 211 (4): 757–63. doi:10.1083/jcb.201505058.

Son, Sungmin, Amit Tzur, Yaochung Weng, Paul Jorgensen, Jisoo Kim, Marc W Kirschner, and Scott R Manalis. 2012. "Direct Observation of Mammalian Cell Growth and Size Regulation." *Nature Methods* 9 (9): 910–12. doi:10.1038/nmeth.2133.

Sung, Yongjin, Amit Tzur, Seungeun Oh, Wonshik Choi, Victor Li, Ramachandra R Dasari, Zahid Yaqoob, and Marc W Kirschner. 2013. "Size Homeostasis in Adherent Cells Studied by Synthetic Phase Microscopy." *Proceedings of the National Academy of Sciences of the United States of America* 110 (41): 16687–92. doi:10.1073/pnas.1315290110.

Taheri-Araghi, Sattar, Serena Bradde, John T. Sauls, Norbert S. Hill, Petra Anne Levin, Johan Paulsson, Massimo Vergassola, and Suckjoon Jun. 2015. "Cell-Size Control and Homeostasis in Bacteria." *Current Biology* 25 (3). Elsevier Ltd: 385–91. doi:10.1016/j.cub.2014.12.009.

Talia, Stefano Di, Jan M Skotheim, James M Bean, Eric D Siggia, and Frederick R Cross. 2007. "The Effects of Molecular Noise and Size Control on Variability in the Budding Yeast Cell Cycle." *Nature* 448 (7156): 947–51. doi:10.1038/nature06072.

Turner, Jonathan J, Jennifer C Ewald, and Jan M Skotheim. 2012. "Cell Size Control in Yeast." *Current Biology* 22 (9). doi:10.1016/j.cub.2012.02.041.Cell.

Tzur, Amit, Ran Kafri, Valerie S Lebleu, Galit Lahav, and Marc W Kirschner. 2009. "Cell Growth and Size Homeostasis in Proliferating Animal Cells." *Science (New York, N.Y.)* 325 (5937): 167–71. doi:10.1126/science.1174294.

Voorn, W. J., and L. J H Koppes. 1998. "Skew or Third Moment of Bacterial Generation Times." *Archives of Microbiology* 169 (1): 43–51. doi:10.1007/s002030050539.

Wallden, M., D. Fange, E. Gregorsson Lundius, Ö. Baltekin, and J. Elf. 2016. "The Synchronization of Replication and Division Cycles in Individual E. Coli Cells (in Press)." *Cell*, 729–39. doi:10.1016/j.cell.2016.06.052.

Wang, Ping, Lydia Robert, James Pelletier, Wei Lien Dang, Francois Taddei, Andrew Wright, and Suckjoon Jun. 2010. "Robust Growth of Escherichia Coli." *Current Biology* 20 (12). Elsevier Ltd: 1099–1103. doi:10.1016/j.cub.2010.04.045.

Zetterberg, A, and D Killander. 1965. "Quantitative Cytophotometric and Autoradiographic Studies on the Rate of Protein Synthesis during Interphase in Mouse Fibroblasts in Vitro." *Experimental Cell Research* 40: 1–11. http://www.sciencedirect.com/science/article/pii/0014482765902843.

Zlotek-Zlotkiewicz, E., S. Monnier, G. Cappello, M. Le Berre, and M. Piel. 2015. "Optical Volume and Mass Measurements Show That Mammalian Cells Swell during Mitosis." *The Journal of Cell Biology* 211 (4): 765–74. doi:10.1083/jcb.201505056.

Figure Legends

Figure 1: Single-cell volume tracking over entire cell division cycles

A) Principle of the fluorescence exclusion-based volume measurement method (FXm). Left: measurement chamber used for 50hrs long time-lapse acquisitions (see SI). Right: principle of the measure. Fluorescence intensity at a point $I_{x,y}$ of the cell is proportional to the height of the chamber minus the height $h_{x,y}$ of the cell at this point. Fluorescence intensity $I_{max}$is the intensity under the known height of the chamber roof h_{max}, where no object excludes the fluorescence. Integration of fluorescence intensity over the cell area gives the cell volume V_{cell} after calibrating the fluorescence intensity signal $\alpha = (I_{max} - I_{min}) \,/\, h_{max}$ (see SI).

B) Sequential images of a HT29 cell acquired for FXm. Mitosis and birth are defined as the time-points 60 min before and 40 min after cytokinesis respectively. The white dashed circle indicates the cell

measured in C), the colored lines indicate the time-points highlighted by circles of the same color in C). Time is in hours:minutes. Scale bar is 20 µm.

C) Single HT29 cell growth trajectory (volume as a function of time) and key measurement points (see SI). ΔT_{tot} is the total duration of the cell division cycle from birth to mitosis and ΔV_{tot} is the total added volume.

D) Average growth speed for three independent experiments with HT29 wild-type cells. n= 39 (exp. 1), n=46 (exp. 2), n=47 (exp. 3). The hinges show the 25th and 75th percentiles and the bars extends from the hinge to the highest value that is within 1.5 * IQR (Inter Quantile Range) of the hinge. The p values are the result of a pairwise t test.

See also Figure S1 and Movie S1

Figure 2: Adder-like behavior in cultured mammalian cells

A) Left: total volume gained during one cell division cycle ΔV_{tot} versus volume at birth V_birth for HT29 expressing hgeminin-mcherry cells. The dashed grey line shows median added volume. Right: volume at mitotic entry $V_{mitosis}$ versus volume at birth V_{birth}. Dashed grey lines show an horizontal line at average volume at mitosis (sizer), and a line of slope 2 with intercept at zero (timer) and slope 1 with intercept at mean volume at birth (adder). a is the slope of a linear fit on the binned data weighted by the number of observations in each bin (see SI), with 95% confidence interval and R2 is the coefficient of determination.

B) Left graph: comparison of rescaled volume at mitotic entry versus rescaled volume at birth for various cultured mammalian cell lines. Ideal curves for stereotypical homeostatic behaviors are shown as black lines. Right table: a, b, CI a (95% confidence interval for a) from linear regressions on binned data for $V_{mitosis} = a.V_{birth} + b$. HT29 are human colon cancer epithelial cells (wild-type (HT29-wt) or expressing hgeminin-mcherry (HT29-hgem)), HeLa are human cervix epithelial cancer cells (either stably expressing MyrPalm-GFP and Histon2B-mcherry (HeLa-MP) or hgeminin-GFP (HeLa-hgem)), MDCK expressing MyrPalm-GFP (MDCK-MP) are dog kidney epithelial cells, Raji are human B lymphoblastoid cells, L1210 are mouse lymphoblastoid cells from data kindly sent by Son and colleagues (Son et al. 2012). Apart from the L1210 cells buoyant mass, data are volumes acquired with either the FXm or the micro-channel methods (See C)).

C) Top: scheme of a cell confined in a micro-channel (nucleus in red). Bottom: sequential images of an asymmetrically dividing HeLa cells expressing MyrPalm-GFP (plasma membrane, green) and Histon2B-mcherry (nucleus, red) growing inside a micro-channel. The outlines of the cell of interest and its daughters (white bars) are shown with white dotted lines. Scale bar is 20 µm. Time is hours:minutes.

D) Ratio of volume in pairs of sister cells at birth and mitosis for MDCK cells expressing MyrPalm-GFP (MDCK-MP) and HeLa cells expressing MyPalm-GFP and Histon2B-mcherry growing inside micro-channels (HeLa-MP). Control, in non-confined condition, corresponds to HeLa expressing hgeminin-GFP (HeLa-hgem) cells measured with FXm. A Wilcoxon signed rank test was performed to test that median was lower from birth to mitosis in each condition. The upper and lower hinges of the boxplot represent the 25th and 75th percentile, the bars extend from the hinge to the highest (lowest) value within 1.5*IQR (Inter Quantile Range) of the hinge. Data beyond the whiskers are shown as outliers.

See also Figure S2 and Movie S2

Figure 3: For HT29 cells, G1 duration is anticorrelated to V_birth

A) Sequential images of HT29 cells expressing hgeminin-mcherry (top) and FXm on the same cells (bottom). The graph on the right shows the quantification of hgeminin-mcherry in the cell as a function of time. Time zero corresponds to cytokinesis (see SI). The vertical white line and arrows indicate the time at which hgeminin-mcherry becomes detectable. G1 phase (red line) spans from birth to appearance of hgeminin (G1/S transition) and S-G2 phases (green line) from G1/S to next entry in mitosis (see SI). Scale bar is 20µm. Time is in hours:minutes.

B) Total added volume ΔV as a function of initial volume for total cycle (blue), G1 (red) and S-G2 phases (green). Dashed blue line indicates the median volume added. Boxes show medians of bins with standard deviation. Pearson's correlation coefficient (P), for the entire cell division cycle: P=0.13, p=0.12, n=141; G1: P=-0.30, p=9*10^-7, n=241; S-G2: P=0.34, p=1*10^-5, n=144; linear regression on the median bins weighted by the number of observations in each bin, G1: a= -0.30+/-0.009, p=1*10^-91, R2=0.83; S-G2: a=0.3+/-0.01, p=3*10^-53, R2=0.83.

C) Histogram of ΔT_{G1} (red) and ΔT_{S-G2} (green). CV: coefficient of variation. Standard deviations are significantly different (Fligner-Killeen test, p=2*10^-16).

D) Duration of G1 phase, ΔT_{G1}, and S-G2 phase, ΔT_{S-G2} versus size at birth, V_birt V_{birth}h. Pearson's correlation coefficient, G1: P=-0.33, p=7*10^-10 (n= 310); S-G2: P=-0.12, p=0.07. (n=220); linear regression on the median bins weighted by the number of observations in each bin, G1: a=-0.008+/-0.0001, p=1*10^-160, R2=0.92; S-G2: a=-0.004+/-0.0001, p=9*10^-4, R2=0.07. Red dashed line and grey area are a visual guide for minimum G1 duration around 4-5 hours.

E) Cumulative frequency graph of ΔT_{G1} binned for three ranges of volumes at birth V_{birth}. Red dashed line and grey area are a visual guide for minimum G1 duration around 4-5 hours.

All data in the figure are from HT29 cells expressing hgeminin-mcherry (N=4).

See also Figure S3 and Movie S3

Figure 4: Larger cells obtained after Roscovitine treatment still display an adder behavior

A) Examples of single-cell growth trajectories for HeLa cells expressing hgeminin-GFP, either control, or after washout from Roscovitine treatment (darker color) as a function of time from birth; G1 is in red and S-G2 in green.

B) G1 duration, ΔT_{G1}, as a function of volume at birth for control (light red, light grey) and Roscovitine-treated cells (darker red, darker grey). Individual cell measures (dots) as well as median of bins (squares) and standard deviation (bars) are shown. Red lines shows linear regression on median bins weighted by the number of event in each bin (control cells: a=-0.00188+/0.00008, R2=0.76, p=5*10-

61; rosco: a=-0.0002±0.0001, R2=0.05, p=1*10-42; Pearson's correlation coefficient, control: P=-0.4, p=3*10^-8, n=199, N=2; Roscovitine: P= -0.03, p=0.8., n=120, N=3). Note that control HeLa cells are already very close to the minimum G1 duration compared to the HT29 cells shown in Figure 3. Distributions on the top are the distribution of volume at birth V_birV_{birth}th; control: mean volume at birth=1600µm3, n=231; rosco: mean volume at birth=2600µm3, n=136; Welch t test comparing the means: p=2.2*10^-16. Distributions on the right are G1 duration: control: mean G1 duration=7.0 hrs, n=201; rosco; mean G1 duration=6.1 hrs, n=124; Welch t test comparing the means: p=6.5*10^-7. Red dashed line and grey area are a visual guide for minimum G1 duration around 4-5 hours.

C) Added volume in G1 (ΔV_{G1}) versus volume at birth for control (light red, light grey) and Roscovitine-treated cells (darker red, darker grey). Individual cell measures (dots) as well as median of bins (squares) and standard deviation are shown. Pearson's correlation coefficient, control: P=-0.06, p=0.4, n=178, N=2; rosco: P=-0.07, p=0.8, n=108, N=3. Dashed lines represent the mean added volume in each condition, control: mean added volume in G1=350 µm3; rosco: mean added volume in G1=390 µm3; Welch's t.test comparing the means, p=0.2423.

D) Instantaneous growth speed ∂v/∂t in G1 as a function of volume, for control (light red squares, n cells=119) and Roscovitine treated cells (dark red triangles, n cells=49). Growth speed was estimated on sliding windows of 90 min (see SI). Red lines shows linear regression on average bins weighted by the number of event in each bin (control: a=0.0489+/-0.0005, p≈0, R2=0.78; rosco: a=0.047+/-0.002, p=2*10^-137, R2=0.49). Grey lines represent bivariate kernel densities.

E) Top: kernel density of volume at birth for control and Roscovitine treated cells together. The 20% and 80% percentiles are represented (the x axis is common to both plots). Bottom: Same data as D) but cells are grouped by their initial volume at birth (cells within the 0 to 20% percentile (blue), 20 to 80% percentile (orange) and 80 to 100% percentile of the distribution (green). The dots represent the averaged bins which contain measurements on at least 5 different cells, the lines are robust linear fits on the bins (0-20%: a=0.13+/-0.05, p=0.0219, R2=0.95; 20%-80%: a=0.084+/-0.02, p=0.000751, R2=0.68; 80%-100%: a=0.081+/-0.009 p=8*10^-7, R2=0.92).

All data are from HeLa cells expressing hgeminin-GFP (control: N=2, Roscovitine: N=3).

See also Figure S4 and Movie S4

Figure 5: Contribution of growth and time modulation in overall size control

A) Doubling rate, log(Vmitosis/Vbirth) versus logarithm of initial volume log(Vbirth) for HT29 wild-type cells. The linear regression (performed on the median bins, blue squares, and weighted by the number of observations in each bin) gives the overall strength of control, λ (-λ =0.5±0.002, R2=0.85, n=132, N=3). Error bars represent standard deviation.

B) Cell cycle duration τ versus initial volume log(Vbirth) for HT29 wild-type cells. The linear regression (performed on the median bins, blue squares, and weighted by the number of observations in each bin) gives the strength of control by time, θ, such that a positive value corresponds to a positive effect on size control (-θ =7±0.2, R2=0.88, n=163, N=3). Error bars represent standard deviation.

C) Growth rate α versus initial size log(Vbirth), for datasets on bacteria, from (Wallden et al. 2016). The linear regression (performed on the median bins, orange squares, and weighted by the number of observations in each bin) gives the control due to growth rate modulations, γ, such that a positive value corresponds to a positive effect on size control (-γ =0.0005±0.0002, R2=0.06, n=2107).

D) Left: plot of θ multiplied by the average time and the average growth rate, versus – γ multiplied by by the average time and the average growth rate (such that a positive value corresponds to a positive effect on size control) for the dataset shown in C for bacteria. Right: plot of θ multiplied by the average growth, versus γ multiplied by average growth for HT29 cells (right). The dashed lines indicate the threshold above which time modulation (horizontal line) and growth modulation (vertical line) have a positive effect on size control.

E) Comparison of datasets for bacteria (data from (Wallden et al. 2016; Kennard et al. 2016; Taheri-Araghi et al. 2015; Kiviet et al. 2014)) and yeasts (data from (Soifer et al. 2016; Nobs and Maerkl 2014)), plotted as in D. The dashed lines indicate the threshold above which time modulation (horizontal line) and growth modulation (vertical line) have a positive effect on size control.

F) Comparison of datasets for eukaryotes (our results and data from (Son et al. 2012)), plotted as in D. The dashed lines indicate the threshold above which time modulation (horizontal line) and growth modulation (vertical line) have a positive effect on size control.

See also Figure S5

FIGURE 1

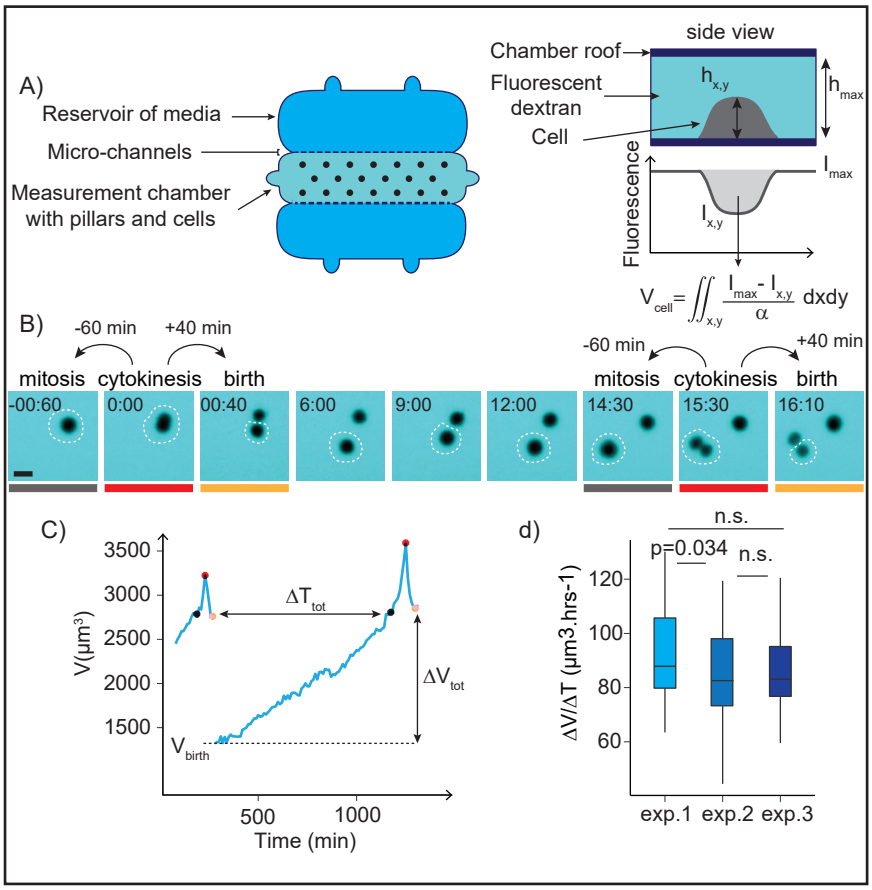

FIGURE 2

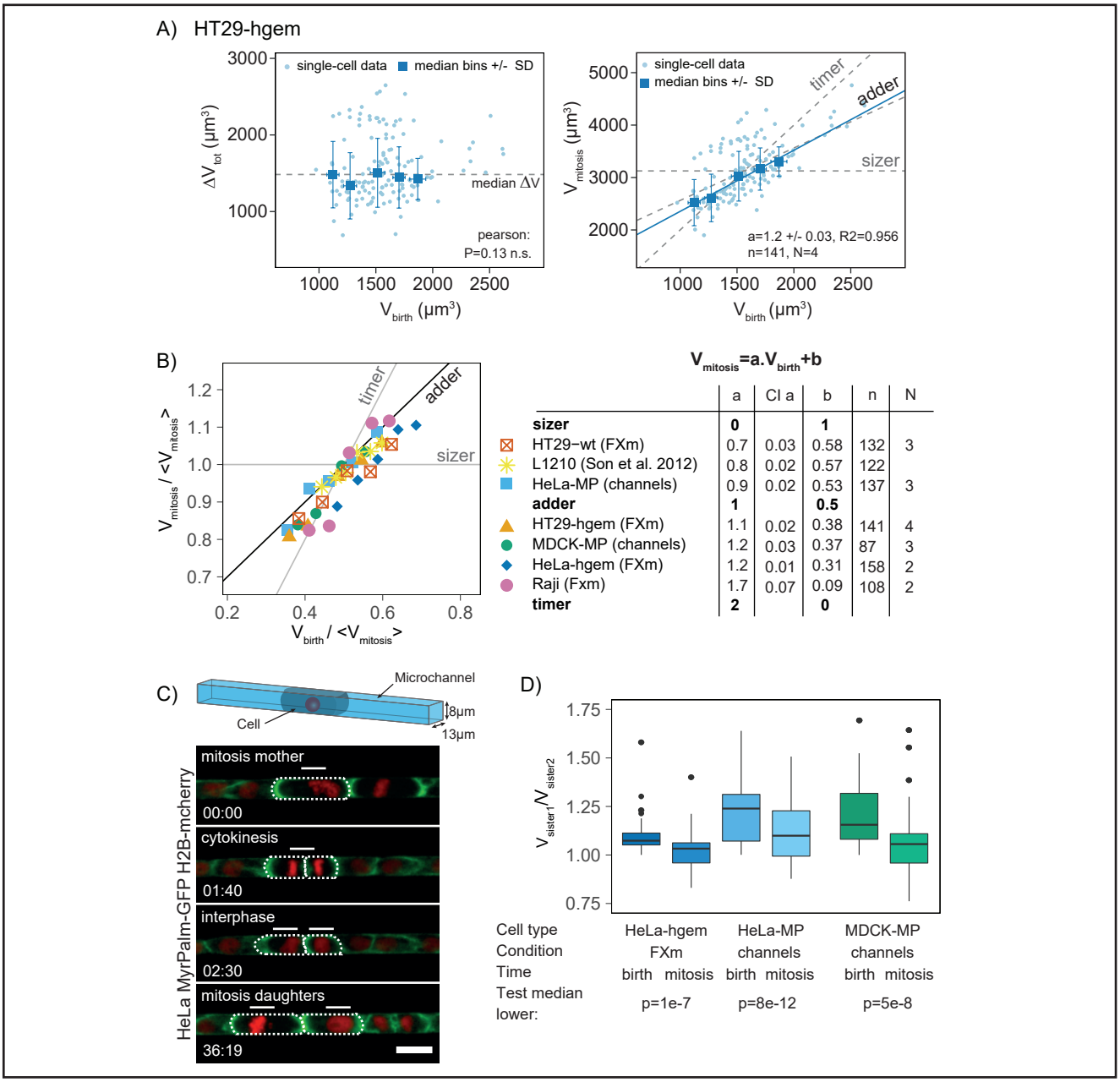

FIGURE 3

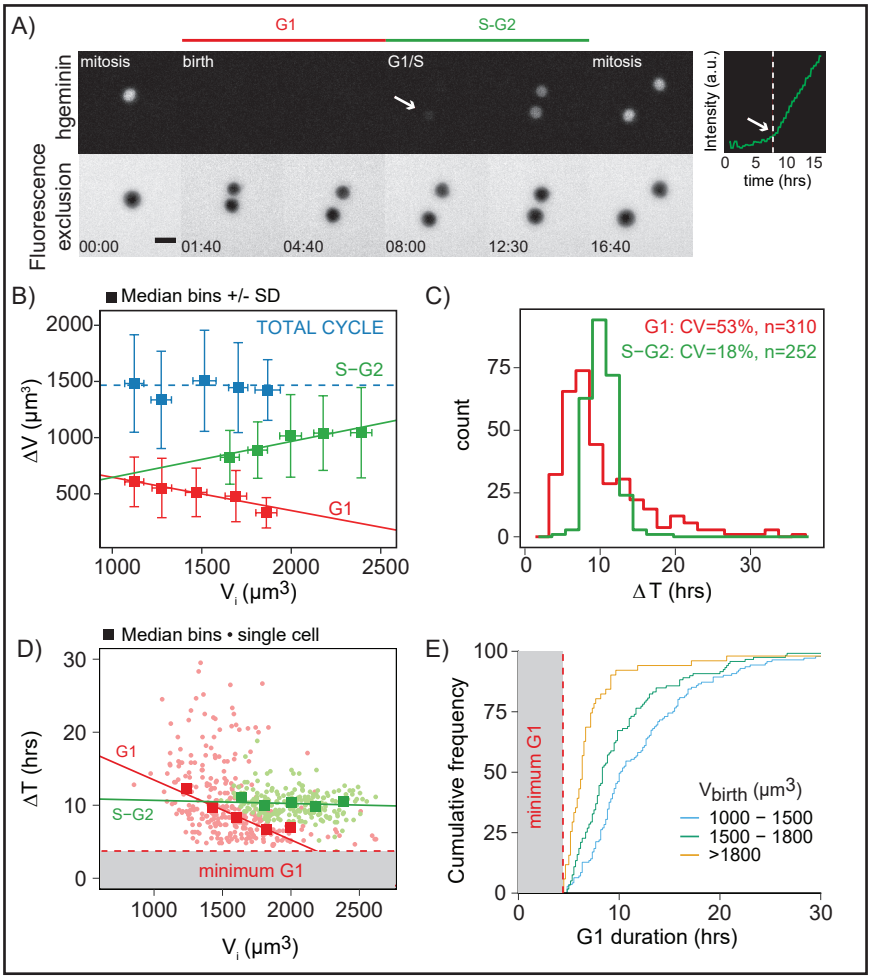

FIGURE 4

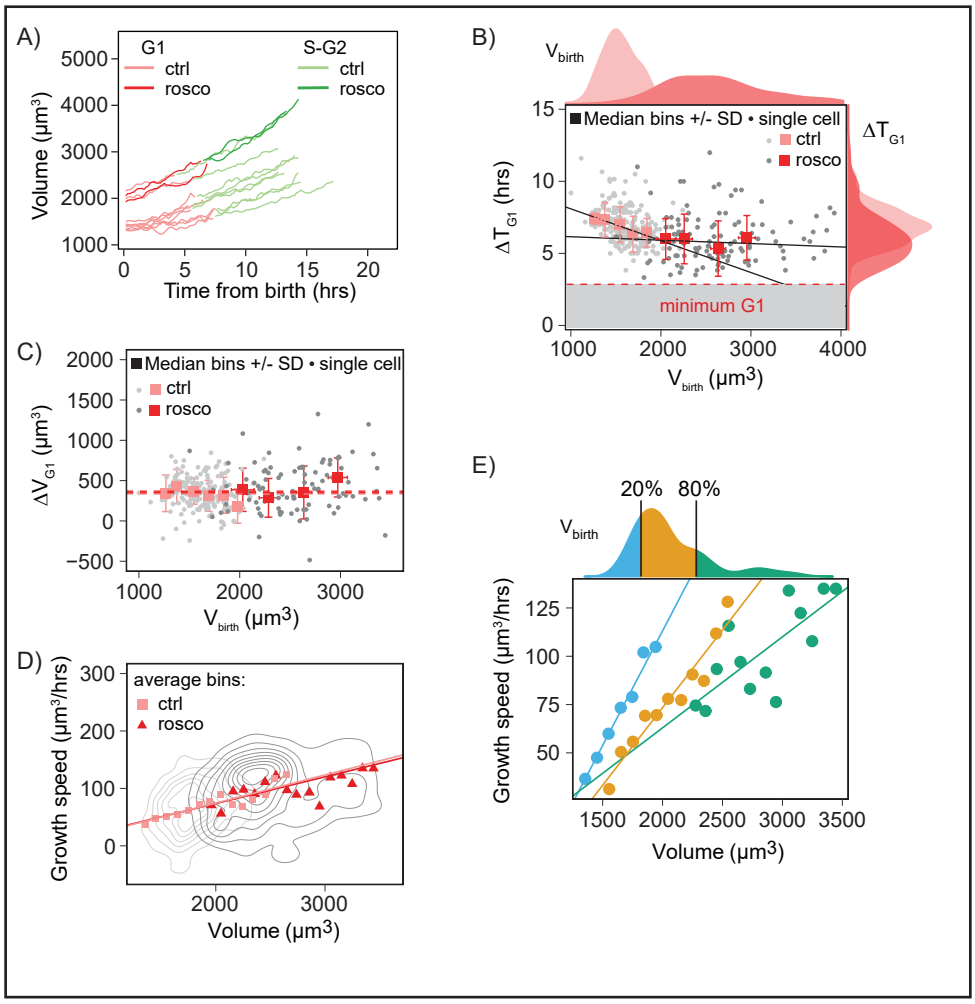

FIGURE 5

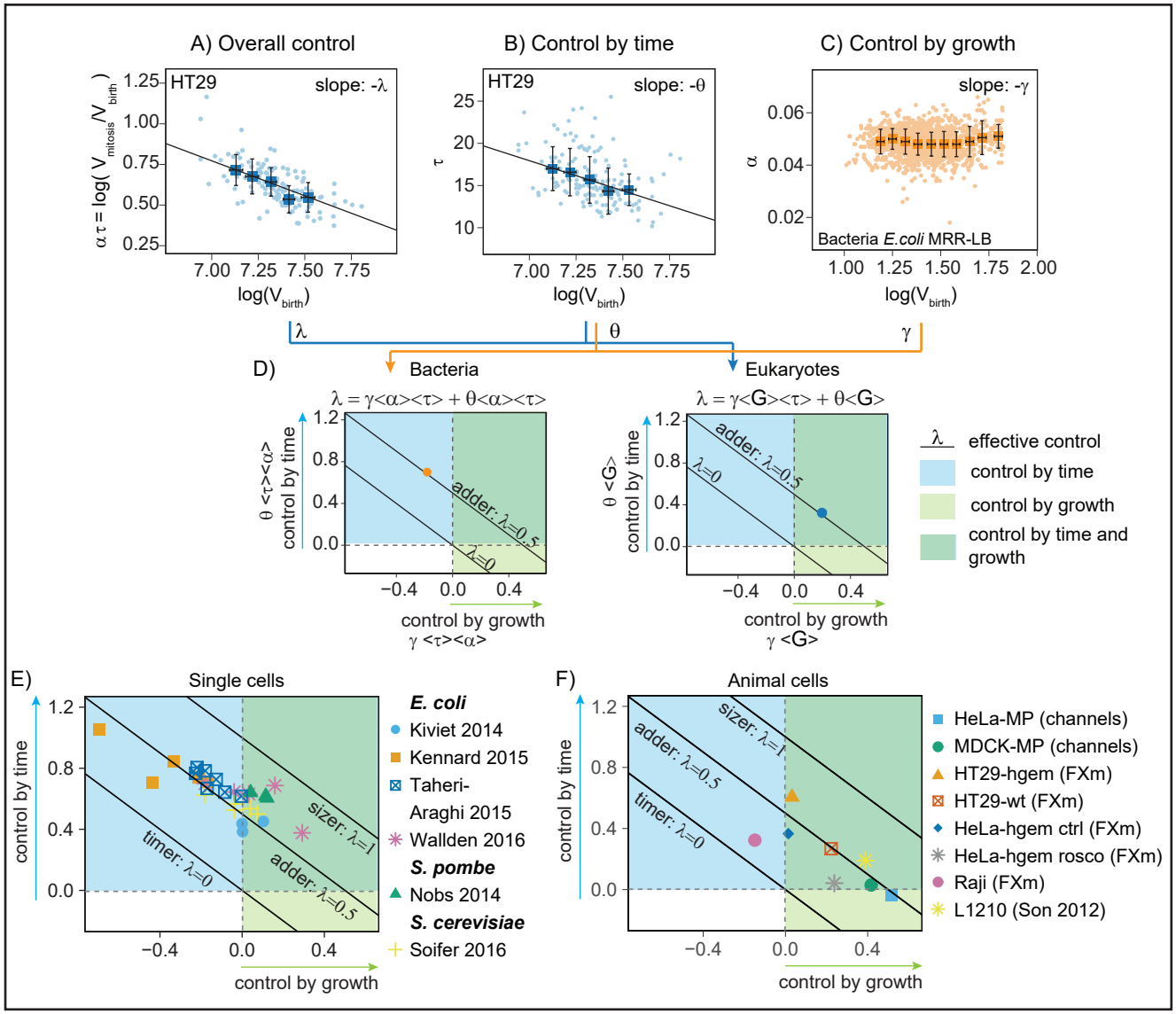

Supplemental information

Material and methods

Cell culture & reagents

Cells were cultured in media supplemented with 10% FBS and 1% penicillin-streptomycin. Media, EDTA, trypsin, penicillin-streptomycin and glutamax were purchased from ThermoFisher. For HeLa, MDCK, HT29, cell culture medium was DMEM-GlutaMAX (HeLa, MDCK, HT29) and medium for microscopy imaging was DMEM with no phenol red (#31053044) supplemented with Glutamax (#35050061). For Raji cells, medium used was RPMI supplemented with GutaMAX #35050061. Zeocin (#10072492) was purchased from Life Technologies and Puromycin (#BML-GR312-0050) from Enzo life sciences. Dextran (#D-22910, #D-22914) and roscovitine (#R7772-1G) were purchased from Sigma Alrich. The stock solution of dextran was 10mg/mL in PBS, the stock solution of Roscovitine was 50mM in DMSO.

Cell lines and plasmids

HeLa cells are human cancerous epithelial cells from adenocarcinoma. HeLa expressing hgeminin-GFP (HeLa-hgem) were a kind gift from Buzz Baum's lab (UCL, London, United Kingdom). HeLa Kyoto expressing MyrPalm-mEGFP-H2B-mRFP (HeLa-MP) are a kind gift from Daniel Gerlich's lab (ETH, Zurich, Switzerland). HT29 cells are human cancerous cells coming from colorectal adenocarcinoma. HT29 wild type cells (HT29-wt) were HT29 HTB-38 were bought from ATCC. A stable HT29 cell line expressing hgem-mcherry (HT29-hgem) was established using the lentiviral vector mCherry-hGeminin(1/60) / pCSII-EF (Sakaue-Sawano et al. 2013): electroporation was used to transfect the cells, the cells were then selected with zeomycin 200µg/mL and FACS-sorted for mCherry fluorescence. The resulting polyclonal population showed a good homogeneity in fluorescence intensity. MDCK cells are dog epithelial cells from an apparently normal kidney. They are however hyperdiploid with a modal chromosome number ranging from 77 to 80 or 87 to 90 (instead of 78 for this specie). MDCK cells were obtained from Buzz Baum lab (UCL, London, United Kingdom). Similarly to the protocol used for HT29 expressing hgem-mcherry, a stable MDCK cell line expressing MyPalm-GFP (MDCK-MP) was established by electroporating cells with the plasmid pMyrPalm-mEGFP-IRES_puro2b offered by Daniel Gerlich's lab. Selection was made with Puromycin 2µg/mL prior to FACS sorting. For all the transfected cell lines, antibiotic were removed from the culture media after FACS sorting. Raji cells are human B lymphoblastoid cells coming from a lymphoma. Raji were obtained from Claire Hivroz's lab (Institut Curie, Paris, France).

Roscovitine experiment

For the roscovitine experiments, HeLa cells were seeded in six-well plates at 1.9*10^4 (control) and 8.3*10^4 (treated) cells per cm2 52 hours before the experiment. 4 hours later (48 hours before the experiment), when cells were spread, media was changed to 2 mL +/- 20µM roscovitine. Roscovitine stock solution was 50mM in DMSO.

Live-cell imaging

Phenol red-free media was used for FXm experiments. Acquisitions were performed on a Ti inverted (Nikon) or Axio Ob-server microscope (Carl Zeiss) at 37°C with 5% C02 atmosphere, a 10× dry objective

(NA 0.30 phase) for FXm experiments or a 20× dry objective (NA 0.45 phase) for micro-channels experiments. Images were acquired using MetaMorph (Molecular Devices) or Axio Vision (Carl Zeiss) software. The excitation source was systematically a LED for FXm experiments to obtain the best possible homogeneity of field illumination (Lumencor or Zeiss Colibri); or a mercury arc lamp for some of the microchannel experiments. Images were acquired with a CoolSnap HQ2 camera (Photometrics) or an ORCA-Flash4.0 camera (Hammamatsu).

For timelapse experiment, images were acquired every 5min (microchannel experiments), 10min (FXm measurements: fluorescence-exclusion channel and phase channel) and 30min (fluorescent geminin channel) for up to 50hours in order to obtain 1 to 2 full cell cycles per lineage.

Volume measurement with FXm

The FXm method was initially described in (Zlotek-Zlotkiewicz et al. 2015) and a detailed protocol is available in (Cadart et al. 2017)**.** We only describe here specifications from this protocol.

Except for Raji experiments, the design of the volume measurement chamber (Figure 1A) included two side reservoirs that diffused nutrients to cells in the middle of the chamber. Side reservoirs were 400µm high and diffusion to the observation part was achieved through a grid of channels (w=100µm, l=300µm and h=5µm). The height of the chambers was around 20-24µm (depending on the chambers) for HT29 and HeLa cells and 15.5 or 18.2µm for the Raji cells.

The chambers were coated with fibronectin 50µg/mL, and then incubated overnight with the appropriate phenol-red-free media. During the acquisition, the chambers were covered with media to prevent desiccation of the PDMS and subsequent changes of the osmolarity of the media in the chamber. To prevent dextran leakage outside the chambers, the height of the inlets was risen by sticking 3-4 mm high PDMS cubes on top of each inlet, then 2mm diameter punches were made for every inlets.

To prevent potential sources of variability in the growth rate or doubling rate caused by different proliferative states in the population, cells were seeded at constant concentration two days before the experiment (1*10^5/cm² for HT29 cells and 1.9*10^4/cm² for HeLa). Cells were detached using trypLE (thermofisher #12605036) (HT29) or EDTA (Life Technologies #15040-033) (HeLa), to avoid cell aggregates and optimize adhesion time to the glass-bottom, fibronectin-coated chamber. Cells were injected in the middle part of the chamber (Figure 1A) at a concentration ranging from 1.5 to 2*10^5 cells /mL in order to obtain the appropriate density in the chambers. For adherent cells (HT29 and HeLa), 4 hours after seeding, media was changed with equilibrated media containing 1mg/mL of 10kDa-Dextran. Raji cells were injected together with the Dextran at the same concentration. 10kDa Dextran could be coupled either to Alexa-645 (HeLa-hgem experiments) or Alexa-488 (all other experiments). Imaging started 2 to 4 hours after changing the media to give time to for media to equilibrate in the chamber and avoid possible inhomogeneity of dextran just after injection.

We checked that cell cycle time was similar inside and outside the measurement device (Figure S1C) and that, for each experiment, volume at birth and the average growth speed was constant throughout the experiment (Figure S1H). For one dataset, HeLa-hgem, a small decrease of volume due to dextran uptake was observed. This decrease remains however small (10% after 33 hrs).

For the analysis of the relationships between volume at birth, volume at mitosis and volume at G1/S and the duration or volume gained between two of these time-points, cells were manually tracked. Mitosis was defined as the point occurring 60 minutes prior to cytokinesis and birth as the point occurring 40 minutes after cytokinesis (Figure 1B and S1E). To check that volume at mitosis was measured before the mitotic volume overshoot, we compared the volume measured 100 minutes and 60 minutes before cytokinesis and verified that they were not significantly different (Welch's t test comparing the means: p=0.8229) (Figure S1F). We also checked that the manual segmentation of daughter cells just after division was correct despite the cells being still close to each other's. To do so, we compared the sum of the volumes of the two daughter cells measured separately (Figure S1F, green) with the value obtained when measuring the two cells at once (Figure S1F, orange). These two measurements were not significantly different (Welch' t test comparing the means p=0.8028). G1/S was identified as the first time-point where hgeminin-GFP (HeLa) or hgeminin-mcherry (HT29) was observed (Figure 3A). This point was visually assessed and we checked that this method was correct compared with an assessment from the fluorescence expression profile (Figure S3A). We compared 10 curves and show here the most imprecise evaluation (Figure S3A left), the average type of error observed (Figure S3A middle) and the best evaluation (Figure S3A right). This empirical check shows that on average the error was small.

Micro-channel experiments

Microchannels molds were made with classical lithography technics and then replicated in epoxy molds. Microchannels had a 104µm2 cross-section area (13µm width by 8µm height) (Figure S1B). They were crossed perpendicularly by two large distributing channels (5mm width by 50µm height). The micro-channels chips were replicated in PDMS, plasma-treated, bound to glass-bottom fluorodishes, coated with fibronectin 50µg/mL and incubated over night with the culture media. The large distributing channels were used both to inject the cells and as reservoirs of media. Cells were injected at a concentration of 3.8*10^6/mL, in the upper distributing channel; the dishes were then tilted with the large distributing channels axis parallel to the bench plane. This helped deposing a thin layer of cells at the entry of the micro-channels while minimizing the number of cells injected for nutrient amount economy and appropriate density's sake. The opposing distributing branch contained only media and thus diffused nutrients to the channels. This was indeed important to guarantee enough nutrient stock and good growth conditions throughout the 50hrs of the acquisition in this confined design. Cells were then let to migrate in the microchannels over-night and experiments were started the morning after. Upon mitotic entry, cells round-up and adopt a cylinder shape because of the confinement. The contours of the cells are visualized by imaging of the protein MyrPalm tagged with GFP that labels cell membrane. Volume was calculated by measuring the length (ℓ) of the cell and multiplying it by the channel cross section area (CS): $V \approx \ell . CS$. (Figure S1B). For the analysis, mitosis was defined as the first time-point where the cell rounds-up and displays a cylinder shape and birth was the last time-point after cytokinesis where the cell is still in the shape of a cylinder (Figure 2B). In the channels, cells cycled slower (their average cell cycle duration was, for HeLa-MP: mean=24.9hrs and for MDCK-MP: mean=19.5hrs, by comparison, HeLa-hgem have an average cell cycle duration of 15.2hrs in the FXm device). However, we checked that volume at birth and average growth speed were constant through time in the experiment (Figure S1H), thus meaning that these experiments are a valid data-set for our study.

Image analysis

For FXm experiments, image analysis was performed using a home-made Matlab program described in (Zlotek-Zlotkiewicz et al. 2015). The growth curves were analyzed with an updated version of this program written in collaboration with the company QuantaCell (Cadart et al. 2017). Rapidly, fluorescent signal was calibrated for every time points using the fluorescence intensity of the pillars and around the cell of interest to obtain the linear relationship between height and fluorescence. After background cleaning, the fluorescence intensity was integrated for the whole cell and its surroundings to obtain the cell volume.

For the micro-channels experiments, image analysis was performed on ImageJ.

Data filtering and analysis

For the data on the animal cells obtained by us (or analyzed from (Son et al. 2012)), only clear outliers that were higher or lower than the mean+/-3*SD were removed. This corresponded on average to 0 to 5 points maximum per dataset (each dataset being n>87). These outliers were removed for visual purposes (scale of the plot adapted to the range of the data) and analytical robustness.

For the bacteria and yeast data obtained from previous studies (Kennard et al. 2016a; Kiviet et al. 2014a; Taheri-Araghi et al. 2015; Soifer et al. 2016; Nobs and Maerkl 2014; Wallden et al. 2016), a filter based on the IQR (interquantile range) was performed: cells which log(Vi) and log (Vf) where higher or lower than 1.5*IQR+/-median of log(Vi) and log(Vf) respectively were removed.

The growth curves were obtained from automated tracking of the movies and analyzed as follow. First, all the tracks were visualized to identify the phases in the cell cycle (birth was automatically detected because the tracks split when the newborn cells separated, mitotic volume overshoot indicating the end of the cell cycle was visually assessed from the volume growth curve (see Figure 1C) and G1/S transition was visually assessed as the transition point in the nuclear-hgeminin fluorescence expression curve as shown in Figure S3A). Both complete cell cycle trajectories and uncomplete trajectories that were longer than 5 hours and contained at least one identified cell cycle event (birth, G1/S or mitosis) were kept. Second, clear outliers caused by errors of segmentation were removed using the following filter: for each volume measurement x_i, if $\frac{x_i}{median\ (X_i)} - 1 < 0.004 \times \frac{SD\ (X_i)}{median\ (X_i)}$, the measurement x_i was removed (here, $median\ (X_i)$ and $SD\ (X_i)$ are local median and local standard deviation values estimated on a window of 11 frames centered on x_i). This filter was a good enough to remove only clear outliers (Figure S1G, left). Third, for the local growth speed measurement, the curves were smoothed by performing sliding average on widows of 7 frames (70min). Then the growth speed at each point was the slope of a robust linear fit performed on windows of 9 frames centered on this point (Figure S1G, middle).

Statistical analysis

All the figures and statistical analysis were performed in R. Packages used were: “robust”, “robustbase”,“ggplot2”,”grid”,”gridExtra”,”xtable”,”stringr”,”RColorBrewer”.

For the boxplots, the upper and lower hinges correspond to the first and third quartiles, the upper and lower whiskers extend from the hinge to the highest (lowest) value within 1.5*IQR (Inter Quantile Range) of the hinge. Data beyond the whiskers are shown as outliers.

For the comparison of the variances in Figure 3C, the test was a Fligner-Killeen test because distribution of the variables were non normal and the median were not always equal.

For the plots where a linear relationship was tested, Pearson's coefficient of correlation is indicated together with its p value. When this coefficient was significantly higher than 0.3 (meaning that the relationship tested explained more than 30% of the correlation between the two variables), a linear fit on the median bins, weighted by the number of observed variables in each bins was performed. In this case, the slope coefficient a is indicated, together with its 95% confidence interval (CI), p value and R2. Linear fits were performed using the "robust" package in R. For all the plots except the ones analyzing growth speed as a function of time or size, the bins are median bins along the x axis of the plot, and the bars represent the standard deviation. Bins that contained less than a minimum number of events were removed. The bin number and the minimum size of the bin was adapted to the size of the datasets as follows:

Cell type	n number of events observed	Bin number	Minimum number of events per bin
Animal cells	80-300	8	8
Bacteria cells	<100	8	8
	<1000	10	15
	<5000	13	60
	>5000	15	150

For the plots testing the relationship between growth speed and volume or time (Figure 4D-E and S4D-F), the bins are average bins and bins that contained measurements on less than 5 different cells were removed to avoid low-sampling effects.

Supplementary figures Legends

Figure S1, related to Figure 1

A) Volume distribution for all the cell types analyzed in this study measured with either the FXm or the micro-channels devices (see SI) (kernel density estimation). Cells types are described in SI.

B) Design of the micro-channels: the micro-channels have a cross section of 102 µm2, (h: height, w: width, L: cell length, V: cell volume, CS: cross section, blue: cell membrane, magenta: DNA, green: microtubules, grey bars: microchannels) (see SI, microchannels experiments).

C) Duration of cell cycle length (ΔT_{tot}) inside (n=132, N1) and outside (n=88, N=1) the FXm measurement device for HT29-hgem cells. Cells were plated at approximately the same density. Cell cycle duration is slightly higher outside the device (Welch t test comparing the means: p<2*10^-16), probably due to a faster equilibration of the media in the small volume of the measurement device. This control shows that cells cycle on expected durations in the measurement device.

D) Examples of complete growth curves of single HT29 wild-type cells obtained with the FXm method. The curves start at birth and end at mitosis.

E) Boxplot of the average volumes centered on cytokinesis shows the mitotic volume overshoot (Zlotek-Zlotkiewicz et al. 2015) in HT29 expressing hgeminin-mcherry cells (HT29-hgem n=22, N=1). The coloured time-points correspond to the time-points 100 minutes before (red), 60 minutes before (blue, time-point where mitosis was defined) and 40 minutes after (orange, time-point where birth was defined) cytokinesis. They are compared in Figure S1F.

F) Average volume measured 100 mins before, 60 minutes before and 40 minutes after cytokinesis. For the time-point 40 minutes after cytokinesis, the volume measured when integrating fluorescence intensity under the two daughter cells at once (orange) or under each daughter cell separately (green) is compared (p values are p values from Welch's t test comparing the means).

G) Instantaneous growth speed ($\delta v/\delta t$) as a function of volume of individual or groups of HT29-hgem cells show that growth is superlinear. The instantaneous growth speed is estimated by a linear robust fit of volume vs. time on sliding windows of 5 frames (50 minutes). Red line: linear fit on the median bins weighted by the number of observation in each bin (a=0.0261+/-0.0002, n=3259, p=2*10^-41, R2=0.9).

H) Controls for the quality of growth made for all the experiments described in Figure 2, 3 and 4 performed either with the microchannels (channels) or the volume measurement device (FXm). Plots of volume at birth vs. time at birth and growth speed (volume gained in one cell cycle divided by the cell cycle duration $\mathrm{DV/DT}$) vs. time at birth in the experiment (time = 0min corresponds to the beginning of the image acquisition). The number of observations corresponds to the number of observations for the graph of $\mathrm{DV/DT}$ vs. $\mathrm{T_{birth}}$ where the minimum number of observations were made (e.g. sometimes, volume could not be measured because the cells were too close to each other but cell cycle duration could still be quantified). Pearson's correlation coefficient (P) and p value (p) are indicated. For HeLa-hgem, a significant decrease is observed (linear robust fit: a=-0.15+/-0.02 R2=0.194, p=2*10^-13).

Figure S2, related to Figure 2

A) Plots for each individual cell type analyzed either with the FXm or with the channels devices. The plots show volume at mitosis ($\mathrm{V_{mitosis}}$), total added volume in the cell cycle ($\Delta\mathrm{V_{tot}}$) and total cell cycle duration ($\Delta\mathrm{T_{tot}}$) vs. volume at birth ($\mathrm{V_{birth}}$). For the $\mathrm{V_{mitosis}}$ vs $\mathrm{V_{birth}}$ plot, the dashed line indicates the slopes of timer, adder and sizer as in Figure 2B and the slope coefficient a is indicated together with its p value, R2 and the number of observations. For the plot of cell cycle duration vs. volume at birth, the pearson's correlation coefficient P is indicated together with its p value. For the plot of total added volume vs. volume at birth, the dashed line indicates the median added volume $\Delta\mathrm{V_{tot}}$ and the pearson's coefficient P is indicated together with its p value. The squares represent the median bins and the error bars the standard deviation. The blue lines represent a linear regression on the bins weighted by the number of observation in each bin. For the HT29-hgem cells (first row, also shown in Figure 2A), a small population of cells gained more volume than the average (more than 2000µm3, orange points, n=26, 18% of the cells). A possible explanation is that these cells represent a sub-clone (from this polyclonal population stably expressing hgeminin-mCherry) which had a longer G1 (mean G1 duration, outliers: m=13.2, mean G1 duration, other cells: m=8.7, Welch t.test comparing the means: p=9.5*10^-5; mean S-G2 duration, outliers: m=11.5, mean S-G2 duration, other cells: m=10.1,

Welch t test comparing the means: p=3.2*10^-5). The conclusion form the analysis performed on all the points (Figure 2A) or population after removal of the outliers (Figure S2A, first row) however yields similar results. (p<0.01:**, p<0.001: ***).

B) Volume distribution of HeLa cells confined (HeLa expressing MyrPalm-GFP H2B-mcherry in the microchannels) and unconfined (HeLa expressing hgeminin-GFP with the FXm) at birth and at mitosis. CV indicates coefficient of variation.

Figure S3, related to Figure 3

All the results in this figures S3A to S3H are from experiments in HT29 expressing hgeminin-mcherry (HT29-hgem) (N=4).

A) 3 examples of fluorescence intensity profile of hgeminin-mcherry in HT29 cells over time (from cell birth to cell mitosis). Comparison of the identification of the G1/S transition visually (red line) or from the fluorescence intensity curves (blue).

B) Trends in each phase (G1, S-G2) and total cell cycle (tot) for HT29-hgem experiments for volume added (ΔV), phase duration (ΔT) and volume at the end of the phase vs. volume at the beginning of the phase. Linear fit on the bins weighted by the number of observations. Bars represent the standard deviation. The legend indicates the slope coefficient a +/- the 95% confidence interval, the p value of the slope coefficient and the R2 of the fit, the pearson's correlation coefficient (P) and its p value (n.s. p>0.5, * p<0.5, ** p<0.01, *** p<0.001). For the trend of added volume as a function of volume at entry in the phase, the dashed line indicates the median volume gained in the phase, for the plot of final volume vs. initial volume in the period, the dashed lines indicates the timer ($V_{f\,phase} = 2\,V_{i\,phase}$), the adder ($V_{f\,phase} = V_{i\,phase} + \langle \Delta V_{phase} \rangle$) and the sizer ($V_{f\,phase} = \langle V_{i\,phase} \rangle$) as in figure 2B).

C) Histogram of G1, S-G2 and total cell cycle durations (ΔT). CV: coefficient of variation.

D) Duration of G1 or S-G2 phases (ΔT phase) with respect to total cell cycle duration (ΔT total cell cycle duration) (n=228). G1 duration correlates strongly with total cell cycle duration (Pearson's correlation coefficient P=0.93 p=2*10^-103) while S-G2 duration does less (P=0.51 p=7*10^-17). (Lines represent robust linear fit on the points).

E)- G) Correlations as in figure S3 of (Soifer et al. 2016) to test the existence of a constant volume increment between two G1/S transitions: E) Volume added during S-G2 (mother cell) is positively correlated with volume at birth of the daughter cell and F) volume added during G1 (daughter cell) is negatively correlated with volume at birth (daughter cell). G) We lack sufficient observations of consecutive cell cycles in HT29 to test the correlation of added volume between two G1/S transitions and volume at birth. (Linear fit on the bins weighted by the number of observation in each bin. Bars represent the standard deviation. The legend indicates the slope coefficient a +/- the 95% confidence interval, the p value of the slope coefficient and the R2 of the fit, the pearson's correlation coefficient (P) and its p value (n.s. p>0.5, * p<0.5, ** p<0.01, *** p<0.001)).

Figure S4, related to Figure 4

A) Control of the quality of growth for experiments with Roscovitine-treated HeLa expressing hgeminin-GFP (HeLa-hgem) cells as in Figure S1H: plots of volume at birth (V_{birth}) and average growth speed (volume gained in one cell cycle divided by the cell cycle duration $\Delta V / \Delta T$) as a function of time at birth (T_{birth}) in the experiment (time = 0 min corresponds to the beginning of the image acquisition). The pearson's correlation coefficient is indicated together with the p value.

B) S-G2 duration (ΔT_{S-G2}) as a function of volume at G1/S ($V_{G1/S}$) transition in control HeLa-hgem cells and Roscovitine treated cells (Pearson's correlation coefficient, control: P=-0.53, p=2*10^-14, n=172, N=2; Roscovitine: P=-0.15, p=0.102, n=107, N=3; linear fit on median bins weighted by the number of observations: control: a=-0.002+/-0.0009 p<0.0001, not calculated for Roscovitine condition where the correlation is null). Squares represent the median bins and bars the standard deviation. Right histograms: S-G2 duration is longer for Roscovitine treated cells (Roscovitine: mean=10 hrs; control: mean=8 hrs, Welch t test comparing the mean: p=3*10^-14).

C) Added volume in S-G2 (ΔV_{S-G2}) as a function of volume at G1/S transition ($V_{G1/S}$) in control and Roscovitine treated HeLa-hgem cells (Pearson's correlation coefficient, control: P=-0.10,p=0.19, n=160, N=2; Roscovitine: P=0.12, p=0.22 n=99, N=3;). The median volume added (dashed lines) in Roscovitine treated cells is significantly higher than in control cells (control: mean=900; Roscovitine: mean=1600; Welch t test comparing the means: p=2*10^-16).

D) Instantaneous growth speed $\partial v / \partial t$ in S-G2 as a function of volume, for control (light green squares, n cells=119) and Roscovitine treated cells (dark green triangles, n cells=49). Growth speed was estimated on sliding windows of 90 min (see SI). Green lines show linear regression on average bins weighted by the number of event in each bin (control: a=0.0478+/-0.0003, p≈0, R2=0.86; rosco: a=0.0400+/-0.0010, p=3*10^-256, R2=0.49). Grey lines represent bivariate kernel densities.

E) Instantaneous growth speed $\partial v / \partial t$ during the cell cycle as a function of volume, for control (light blue squares, n cells=119) and Roscovitine treated cells (dark blue triangles, n cells=49). Growth speed was estimated on sliding windows of 90 min (see SI). Blue lines show linear regression on average bins weighted by the number of event in each bin (control: a=0.0559+/-0.000, p≈0, R2=0.92; rosco: a=0.0457+/-0.0006, p≈0, R2=0.69). Grey lines represent bivariate kernel densities.

F) Instantaneous growth speed $\partial v / \partial t$ during the cell cycle as a function of time from G1/S transition in control (left, n cells=1198) and Roscovitine treated cells (right, ncells=49). Growth speed was estimated on sliding windows of 90 min (see SI). Red and Green lines show linear regression on average bins weighted by the number of event in each bin for G1 and S-G2 phases respectively (control, G1: a=8.83+/-0.05, p≈0, R2=0.92; control, S-G2: a=5.26+/-0.05, p≈0, R2=0.66; rosco, G1: a=14.5+/-0.3, p≈0, R2=0.77; rosco, S-G2: a=4.15+/-0.09, p≈0, R2=0.55).

G) Examples showing how single-cell vollume curves were smoothed and growth speed was calculated for one control (top) and one Roscovitine treated cell (bottom). Left: first, outliers (orange points) corresponding to errors in the automated segmentation of the cell were removed from the data (blue points) (see SI for the protocol). Middle: calculation of the instantaneous growth speed. The dark points are the data kept after filtering out the outliers, the small segments indicate the local robust linear fit performed on sliding windows of 1h30 (each window contains 9 points) (see SI). The

segments are colored as a function of the slope of the local fit which indicates the value of the instantaneous growth speed and ranges from 0 to 300µm^3/hrs (scale-bar). Right: growth speed as a function of time. Points are colored as a function of growth speed (scale-bar).

H) and I) Examples of 8 complete single-cell volume curves for HeLa expressing hgeminin-GFP control cells (H) and roscovitine treated cells (I). For each cell, the dark points represent the raw measurement and the vertical line the time of G1/S transition. The segments represent the local robust linear fit performed to estimate the instantaneous growth speed and are colored as a function of the slope of this fit to indicate the local value of growth speed (scale bar).

Figure S5, related to Figure 5

A) Example of the size-growth plot for one mammalian cell type (HT29 wild type) and one dataset from a study in bacteria (Wallden et al. 2016). The slope -λ indicates the strength of effective size control. Linear fit on the median bins weighted by the number of observations in the bins. Bars represent the standard deviation.

B) Example of the plot testing the control by time modulation in one of our dataset (HT29 wild type) and one dataset from a study in bacteria (Wallden et al. 2016). The slope -θ indicates the part of size control that is due to modulations of time. Linear fit on the median bins weighted by the number of observations in the bins. Bars represent the standard deviation.

C) Example of a plot testing the control by growth rate modulation in one of the dataset from a study in bacteria (Wallden et al. 2016). The slope –γ indicates the part of size control that is due to modulations of growth rate. Linear fit on the median bins weighted by the number of observations in the bins. Bars represent the standard deviation. For animal cells and data in yeasts, γ is indirectly calculated from the values of λ, θ and <G>, the average size doubling.

D) Comparison of the estimation of the values of λ and θ using a calculation of the covariance (see SI) or a linear fit on the binned data (see SI and above Figures S5A-B). Top: datasets from bacteria and yeasts studies (Wallden et al. 2016; Kennard et al. 2016; Taheri-Araghi et al. 2015; Kiviet et al. 2014; Nobs and Maerkl 2014; Soifer et al. 2016), bottom: datasets from our experiments and on L1210 (kindly sent by (Son et al. 2012).

E) Validation of the model using bacteria: comparison of γ as predicted by the model (see SI) with γ calculated from a fit on the bins (as in Figure 5C). The line represents the relation y=x.

F) Same results as in Figure 5E for bacteria datasets but with the normalization of γ and θ with average doubling $\langle G \rangle$ instead of the product of average growth rate $\langle \alpha \rangle$ and average cell cycle duration $\langle \tau \rangle$ as was used for mammalian cells and yeasts results (where the average growth rate $\langle \alpha \rangle$ is not available) (see SI).

G) Results as in Figure 5E with the detail of the growth condition for each dataset analyzed for yeasts and bacteria. For more precisions about the experimental conditions, please refer to the corresponding publications (Kiviet et al. 2014; Nobs and Maerkl 2014; Kennard et al. 2016; Soifer et al. 2016; Taheri-Araghi et al. 2015; Wallden et al. 2016). It is worth noting that *S. pombe*, although it

is long known to display a strong size control through the existence of a size-checkpoint that delays mitotic entry (Turner, Ewald, and Skotheim 2012) shows an effective size control slightly less efficient than a pure sizer. This is in fact explained by the fact that the negative correlation between cell cycle duration and size at birth reaches a plateau for very large sizes, an observation long reported for this cell type (Fantes 1977) and reproduced with the dataset analyzed here (Figure 6 of (Nobs and Maerkl 2014)). In other words, in *S. pombe* similarly to our observation in large Roscovitine treated cells, the existence of a minimal cell cycle duration limits the time-dependent size correction mechanism for very large cells and the effective size homeostasis behavior is not strictly an adder.

H-J) Correlation between the duration of S-G2 (ΔT_{S-G2}) and the duration of G1 phase (ΔT_{G1}) in: G) HT29 wild-type, H) HeLa-hgem control and I) HeLa-hgem Roscovitine treated. Linear fit on the median bins weighted by the number of observation in each bin, bars represent the standard deviations, squares the median bins.

Suplementary movies

Movie S1, related to Figures 1A-B

Long time-lapse acquisition in the FXm device of HT29 expressing hgeminin-mcherry, HeLa expressing hgeminin-GFP and Raji cells. The images show a full field acquired in 10X, dark pillars or area are the pillars that sustain the roof of the chamber at a constant height (see Figure 1A), the culture medium contains a fluorescent dye (Dextran 10kDa coupled to Alexa488 or Alexa 647). Time is in hrs:min. frame rate is 10min, total acquisition length are 50hrs (HT29-hgem), 19h50 (HeLa-hgem), 39h30 (Raji), scale bar is 100µm.

Movie S2, related to Figure 2C

Long time-lapse acquisition of HeLa expressing MyrPalm-GFP (membrane) and H2B-mcherry (DNA) in micro-channels of cross section 102µm2. Time is in hrs:min. frame rate is 5min, total acquisition length is 43h15min, scale bar is 20µm.

Movie S3, related to Figure 3A

One complete cell cycle of a HT29 cell expressing hgeminin-mcherry in FXM device. Left field shows images obtained with FXm, right field shows hgeminin-mcherry signal. Time is hrs:min, frame rate is 10min, total length of the movie is 18h40, scale bar is 20µm.

Movie S4, related to Figure 4

Control (top) and Roscovitine-treated (bottom) HeLa cells expressing hgeminin-GFP in FXm device. For each cell, the movie starts 1 time-point (10min) before cytokinesis of the mother cell and stops 4 time-points (40min) after cytokinesis of the two daughter cells. Time is hrs:min, frame rate is 10min, scale bar is 20µm.

References

Sakaue-Sawano, A., T. Hoshida, M. Yo, R. Takahashi, K. Ohtawa, T. Arai, E. Takahashi, S. Noda, H. Miyoshi, and A. Miyawaki. 2013. “Visualizing Developmentally Programmed Endoreplication in Mammals Using Ubiquitin Oscillators.” *Development* 140 (22): 4624–32. doi:10.1242/dev.099226.

Supplementary Note on the mathematical framework for comparing size homeostasis mechanisms in various organisms

I. BRIEF INTRODUCTION

The correlation pattern of measured variables such as cell sizes, growth rate or growth speed across well-defined cell-cycle intervals and duration of such intervals contains a wealth of information (arguably all the accessible information) about the underlying homeostatic mechanisms (Osella et al., 2017).

The general patterns of such correlations, as well as the links to the molecular mechanisms are still incompletely understood. A commonly accepted hypothesis in both bacteria and yeasts is that size control relies on an adaptation of cell cycle duration to growth, typically through either a critical size threshold ("sizer") or a critical added size threshold ("adder") (reviewed in (Jorgensen and Tyers, 2004; Jun and Taheri-Araghi, 2015; Mitchison, 2003; Turner et al., 2012)). Indirect evidence supporting this hypothesis has been provided in mammalian cells (Dolznig et al., 2004; Jorgensen and Tyers, 2004; Killander and Zetterberg, 1965) and is further reinforced by our direct observation of a negative correlation between G1 duration and volume at birth (Figures 3D and 4C in Main Text).

The alternative hypothesis that growth is coordinated to cell cycle (Goranov and Amon, 2010) and can be actively modulated to maintain size control (Ginzberg et al., 2015) was long neglected. This is probably due to the fact that growth has in many cases been shown to be well described by a mono-exponential curve, in *E. coli* (Godin et al., 2010; Iyer-Biswas et al., 2014; Osella et al., 2014; Wang et al., 2010), and *S. cerevisiae* (Di Talia et al., 2007; Godin et al., 2010; Soifer et al., 2016) single cells, and also in mammalian cells (Godin et al., 2010; Park et al., 2010; Sung et al., 2013; Tzur et al., 2009). However, recent studies of mammalian cells also argued in favor of a control of cell-cycle progression relying on modulations of growth speed, either based on direct measurements (Son et al., 2012) or indirectly (Kafri et al., 2013; Tzur et al., 2009). Consistent with these studies, we also report that the positive trend between growth speed and volume is smaller for cells that are larger at birth, and large for those that are born smaller (see Figure 4E in the Main Text, and the discussion of our experiments on Roscovitine-treated HeLa-hgem cells).

To investigate the interplay between these two distinct mechanisms, it is useful to develop a simple data-analysis approach able to quantify their relative contributions to cell size control. The following sections define a simple mathematical modeling framework that addresses this issue, and is in principle applicable to both the whole cell cycle and to specific cell-cycle stages.

II. MODEL INGREDIENTS

Motivated by the fact that linear correlations are able to explain most patterns in existing data we follow the framework of refs. (Amir, 2014; Grilli et al., 2017), where size homeostasis is represented as a linear correction to perturbations in logarithmic size and exponential growth rate. Each cell is born with a certain size. Its interdivision time or cell-cycle stage duration has an intrinsic stochasticity and may be chosen based on initial

size. Its growth is represented as an exponential growth rate α and a cell-cycle (or cell-cycle subperiod) timing τ, which may be coupled to size. Under these assumptions, the final volume (in a cell cycle or subperiod) is represented as the result of a size-dependent growth and timing

$$V_f = V_0 \exp\left[\alpha(V_0)\tau(V_0,\alpha)\right] \ , \tag{1}$$

where V_x is volume (see also Table I for variable definitions. Here, α and τ quantify the growth rate and duration in the period (or cell cycle) and they are both random variables. For convenience, we define $q_x = \log(V_x)$ and consider the fluctuations of logarithmic size. The overall multiplicative growth of a cell in one cycle is quantified by $G = q_f - q_0 = \log \frac{V_f}{V_0} =: \alpha\tau$.

Note that this framework does not formally require the hypothesis of exponential growth, but just states that growth during a period or a cell cycle is represented as a product of the time interval and an effective (exponential) rate. However, for cells that grow sub-exponentially, the variable α carries a natural dependency on τ which makes interpretation more complex. In brief, for non-exponential growth rate, the contribution of growth rate to size-homeostasis may be a sum of two components, (i) an active size-based compensation of the speed of growth, for example smaler cells at a certain checkpoint decide to accelerate, etc. and (ii) a passive basal mode of growth, e.g. linear growth (see section V below, which explicitly addresses this question within the model framework).

Variable	*Description*	*Definition*
t	time	
V_0	volume at birth	
$V(t)$	volume at time t	
V_f	volume at division	
τ	time at division	
α	growth rate	see Eq. 1
$\langle\alpha\rangle$	average growth rate	
δ_α	growth rate fluctuations	$\delta_\alpha = \alpha - \langle\alpha\rangle$
q_0	logarithm of the initial volume	$q_0 = \log(V_0)$
$\langle q_0\rangle$	average of q_0	
σ_q^2	variance of q_0	
q_f	logarithm of the volume at division	$q_f = \log(V_f)$
δ_q	initial volume log fluctuations	$\delta_q = q_0 - \langle q_0\rangle$
G	overall multiplicative growth	$G = q_f - q_0 := \alpha\tau$
φ_τ	relative contribution of δ_q to fluctuations of the divison time	see Eq. 2
T_τ	relative contribution of δ_α to fluctuations of the divison time	see Eq. 2
φ_G	relative contribution of δ_q to fluctuations of G	see Eq. 3
T_G	relative contribution of δ_α to fluctuations of the divison time	see Eq. 3
γ	contribution of δ_q to fluctuations of the growth rate	see Eq. 4
λ	slope of the size-growth plot	see Eq. 5
θ	contribution of δ_q to fluctuations of the division time	see Eq. 6
β	exponent of polynomial growth	see Eq. 8

TABLE I Table of the main variables

III. RELATIVE ROLES OF TIMING AND GROWTH IN SIZE HOMEOSTASIS

This section shows how the homeostatic control strength on overall growth G is a balance of size-based correction by timing (i.e., on τ) and correction by growth-rate modulation (i.e., on α).

Introducing the notation $\delta_q = q_0 - \langle q_0 \rangle$ to represent the initial size fluctuations of a given cell, and $\delta_\alpha = \alpha - \langle \alpha \rangle$, which represents the fluctuations in growth rate, we can write the overall timing as a function of these two fluctuations,

$$\tau - \langle \tau \rangle = -\langle \tau \rangle \left(\varphi_\tau \delta_q + T_\tau \delta_\alpha \right) + \nu_\tau \ , \tag{2}$$

stating that the time interval could be modulated and. Positive values of the coupling constants φ_τ and T_τ indicate a homeostatic correction (e.g. a cell born smaller growing for a longer time), while negative ones stand for noise-increasing ones. These variables quantify the size- and growth-rate based modulation of overall period timing; they are measurable from conditional averages or correlations, similarly to the slope of the size-growth plot. Finally, ν_τ represents the residual noise on the period timing, when the dependencies on the other variables are removed.

Equally,

$$G - \langle G \rangle = -(\varphi_G \delta_q + T_G \delta_\alpha) + \nu_G \ , \tag{3}$$

where analogous varibles and coupling constants have been defined (see Table I). Since $G = \alpha\tau$ and $\alpha = \langle \alpha \rangle + \delta_\alpha$, the two conditions on timing and overall growth have to be related. We can write the overall growth as

$$G = \langle \alpha \rangle \tau + \tau \delta_\alpha = \langle \alpha \tau \rangle - \langle \alpha \rangle \langle \tau \rangle \varphi_\tau \delta_q + \langle \tau \rangle (1 - \langle \alpha \rangle T_\tau) \delta_\alpha + \dots \ ,$$

where we have neglected nonlinear terms and implied noise terms. The above equation gives an equivalence between the coupling parameters for G and for τ, in absence of any control on the growth rate α.

$$\varphi_G = \langle \alpha \rangle \langle \tau \rangle \varphi_\tau$$

and

$$T_G = -\langle \tau \rangle (1 - \langle \alpha \rangle T_\tau) \ .$$

We now deal with the fact that the growth rate fluctuations can also be linked to size fluctuations (figure S5C), i.e.,

$$\alpha - \langle \alpha \rangle = -\langle \alpha \rangle \left(\gamma \delta_q \right) + \nu_\alpha \ . \tag{4}$$

For exponentially growing cells, this equation expresses the fact that for positive values of γ cells that are born (or enter a cell-cycle stage) larger than average can correct their sizes by growing with a slower rate, and cells that are born (or enter a cell-cycle stage) with a smaller size than average can correct by growing at a faster rate. Conversely, for negative values of γ, growth rate variability increases systematically size variability. For sub-exponential growth, these correlated fluctuations can be homeostatic, but they cannot be interpreted as an active size-based correction. The well-known case is that linearly growing cells without any timing correction (i.e., a timer), perform size correction and add an average constant size at every cycle (Conlon and Raff, 2003) A more general case interpolating parametrically linear and exponential growth is discussed in the following section. Nevertheless, our formalism remains valid, and gives a decomposition of size correction into separate contributions due to modulation of timing and of growth rate.

The slope λ of the size-growth plot is computed considering the conditional average of

G over logarithmic size q (Figure S5A),

$$\langle G\rangle_q = \langle G\rangle - \lambda\delta_q \tag{5}$$

Computation of this average gives

$$\langle G\rangle_q = \langle G\rangle - \varphi_G\delta_q - T_G\langle\delta_\alpha\rangle_q = \langle G\rangle - (\varphi_G - \gamma\langle\alpha\rangle T_G)\,\delta_q$$

leading to the relationship

$$\lambda = \varphi_G - \gamma\langle\alpha\rangle T_G$$

In a similar way, if we define the control parameter θ as the slope of the plot of τ *vs* logarithmic initial size (Figure S5B), i.e.,

$$\langle\tau\rangle_q = \langle\tau\rangle - \langle\tau\rangle\theta\delta_q \tag{6}$$

we have that:

$$\langle\tau\rangle_q = \langle\tau\rangle - \langle\tau\rangle\varphi_\tau\delta_q - \langle\tau\rangle T_\tau\langle\delta_\alpha\rangle_q = \langle\tau\rangle - \langle\tau\rangle\,(\varphi_\tau - \gamma\langle\alpha\rangle T_\tau)\,\delta_q\ ,$$

leading to the relationship

$$\theta = \varphi_\tau - \gamma\langle\alpha\rangle T_\tau$$

Using $\varphi_G = \langle\alpha\rangle\langle\tau\rangle\varphi_\tau$ and $T_G = -\langle\tau\rangle(1 - \langle\alpha\rangle T_\tau)$, we obtain

$$\lambda = \langle\alpha\rangle\langle\tau\rangle\varphi_\tau + \gamma\langle\alpha\rangle\langle\tau\rangle(1 - \langle\alpha\rangle T_\tau)$$

And therefore we obtain:

$$\frac{\lambda}{\langle\alpha\rangle\langle\tau\rangle} = \varphi_\tau + \gamma(1 - \langle\alpha\rangle T_\tau) = \varphi_\tau - \gamma\langle\alpha\rangle T_\tau + \gamma\ .$$

Hence, from the measurements of θ and λ, we obtain Equation 1 in the main text:

$$\theta\langle\alpha\rangle\langle\tau\rangle = \lambda - \gamma\langle\alpha\rangle\langle\tau\rangle\ . \tag{7}$$

Quite simply, Eq. (7) states that the overall correction to size over a cell cycle has to be the sum of a correction due to modulation of timing and a correction due to growth rate. The same approach can be readily generalized to a cell-cycle stage.

For the bacteria datasets, both $\langle\alpha\rangle$ and $\langle\tau\rangle$ are accessible, therefore this relationship can be directly tested (Figures 5 and S5A-C). Another (equivalent) consistency test is discussed in the following section. For mammalian cells, since α cannot be measured directly, we use the approximation $\langle\alpha\rangle\langle\tau\rangle \approx \langle G\rangle$ (Figures 5D and S5C). To verify that this approximation was correct, we repeated the analysis shown in Figure 5E in bacteria with this approximate normalization, using $\langle G\rangle$ (Figure S5F). The results were very similar with the two normalizations, except for two datasets coming from (Kennard et al., 2016). A possible explanation for the lack of consistency of these datasets is that they were acquired on agar pads, with more intersected lineages and less steady conditions for growth-division.

IV. TEST OF THE BALANCE EQUATION ON BACTERIA

Both λ and θ can be determined directly from the covariance between measured variables. Since, by definition

$$\langle G \rangle_q = \langle G \rangle - \lambda \delta_q$$

and

$$\mathrm{cov}(G, q) := \langle \langle G \rangle_q \delta_q \rangle \ ,$$

we have that

$$\mathrm{cov}(G, q) := -\lambda \sigma_q^2 \ ,$$

where σ_q^2 is the variance of q. Analogously, we have that

$$\mathrm{cov}(\tau, q) := -\langle \tau \rangle \theta \sigma_q^2 \ .$$

Using the above relationships, we can obtain λ and θ using

$$\lambda = -\frac{\mathrm{cov}(G, q)}{\sigma_q^2} \ ,$$

and:

$$\theta = -\frac{\mathrm{cov}(\tau, q)}{\langle \tau \rangle \sigma_q^2} \ .$$

Figure S5D shows a comparison of the values obtained for λ and θ from either the covariances or a linear fit testing the relationships (equations 5 and 6 respectively). The two methods are in excellent agreement for all data sets (Figure S5D), except HT29-hgem, probably because there of the noise added by the small outlier population (highlighted in orange, Figure S2A). For this cell type, θ was better inferred by a fit on the median bins and this value was thus used for the model in Figure 5F.

Eq. (7) predicts a value of γ using the measured values of λ and θ

$$\gamma_{pred} = \frac{1}{\sigma_q^2} \left(\frac{\mathrm{cov}(G, q)}{\frac{\mathrm{cov}(\tau, q)}{\langle \tau \rangle} - \langle \tau \rangle \langle \alpha \rangle} \right)$$

If individual growth rates are available, as with the bacteria datasets, γ can also be estimated directly as

$$\gamma_{meas} = -\frac{\mathrm{cov}(\alpha, q)}{\sigma_q^2 \langle \alpha \rangle} \ .$$

Supplementary Figure S5E shows that the measured value γ_{meas} and the predicted value γ_{pred} are in very good agreement, as expected from our theoretical considerations.

V. NON-EXPONENTIAL GROWTH

As discussed above, for cells that do not grow exponentially the control parameter γ in Eq. (4) should not necessarily be interpreted as an active modulation of growth rate. This section quantifies the predicted correlations in the case of sub-exponential growth.

A. Linear growth

We start revieweing the case of linear growht. If cells grow linearly, we have that

$$V(t) = V_0 + V_c g t \ ,$$

where g has dimension of the inverse of time and V_c dimension of size. At division we obtain

$$V_f = V_0 + V_c g \tau \ .$$

Note therefore that for cells that grow linearly and devide according to a timer ($\theta = 0$)

$$V_f = V_0 + \Delta V \ ,$$

which correspond to an adder (i.e., $\lambda = 1/2$). Applying equation 7 to this case, one would obtain a value of γ diffenrent from zero, so that the control appears to operate fully through growth-rate modulation (which is correct, as there is no timing modulation for a timer). However, the size correction is not active, since there are also strong correlations between α and τ, since α is defined as $1/\tau \log(V_f/V_0)$ and linear growth ($V_f = V_0 + V_c g \tau$) makes it a function of τ. In other words, in this case one has to be careful not to mistake the intrinsic properties of a timer for a linearly growing cells with an active mechanism of growth modulation.

B. Polynomial growth

We now derive the predicted correlation pattern in the case of more general sub-exponential growth, and in particular for cells whose volume follows the equation

$$\frac{dV}{dt} = g V^{1-\beta} V_c^{\beta} \ . \tag{8}$$

This model reduces to linear growth in the case of $\beta = 1$ and to exponential growth in the case $\beta = 0$, for intermediate cases, growth is polynomial. This growth model depends only on the parameter β and another one effective parameter $g V_c^{\beta}$. We separate the contribution of g (with dimension of the inverse of time) and V_c (with dimension of size). We will show that $\gamma > 0$ (size-restoring growth-based homeostasis) emerges in the case of $\beta > 0$. Hence, sublinear growth may carry some homeostatic control on size.

Defining $q := \log(V/V_c)$ one obtains

$$\frac{dq}{dt} = g e^{\beta q} \ ,$$

whose solution is

$$q(t) = \frac{1}{\beta} \log\left(e^{\beta q_0} + \beta g t\right) \ .$$

We have therefore that final logarithmic size q_f of a cell with initial size q_0 and division time τ is equal to

$$q_f = \frac{1}{\beta} \log\left(e^{\beta q_0} + \beta g \tau\right) \ .$$

As above, we define $G = q_f - q_0$ and, the exponential growth rate α as G/τ. In the case of $\beta = 0$, $g = \alpha$. Our goal is to show that, for $\beta > 0$ a homeostatic control on α

emerges, i.e.,

$$\alpha := \frac{G}{\tau} = \frac{q_f - q_0}{\tau} = \langle \alpha \rangle (1 - \gamma \delta_q) \ ,$$

with $\gamma \neq 0$ for $\beta > 0$.

Here we assume no direct control on g (i.e., it is a constant independent of the initial size) and no dependence of τ on δ_α ($T_\tau = 0$). We have therefore

$$\tau = \langle \tau \rangle \left(1 - \varphi_\tau \delta_q\right) + \nu_\tau \ .$$

Using the definition of $G = q_f - q_0$ and $q_0 = \langle q_0 \rangle + \delta_q$, we have

$$G = q_f - q_0 = \frac{1}{\beta} \log \left(e^{\beta \langle q_0 \rangle + \beta \delta_q} + \beta g \langle \tau \rangle (1 - \varphi_\tau \delta_q) + g \nu_\tau \right) - \langle q_0 \rangle - \delta_q \ ,$$

which, by expanding around $\delta_q = 0$, simplifies to

$$G = \frac{1}{\beta} \log \left(e^{\beta \langle q_0 \rangle} + \beta g \langle \tau \rangle + \beta (1 - g \langle \tau \rangle \varphi_\tau) \delta_q + g \nu_\tau \right) - \langle q_0 \rangle - \delta_q \ ,$$

and then

$$G = \frac{1}{\beta} \log \left(e^{\beta \langle q_0 \rangle} + \beta g \langle \tau \rangle \right) - \langle q_0 \rangle + \left(\frac{1 - g \langle \tau \rangle \varphi_\tau}{e^{\beta \langle q_0 \rangle} + \beta g \langle \tau \rangle} - 1 \right) \delta_q + \text{noise} \ .$$

Since the single-cell growth dynamics is specified by the parameter $g V_c^{1-\beta}$, we are free to choose V_c arbitrarely. V_c enters in the definition of $q_0 = \log(V_0/V_c)$ and sets the value of $\langle q_0 \rangle$. The simplest choice is to consider $\langle q_0 \rangle = 0$. Note that this can be done in full generality, as it only affects the definition of g in the case $\beta > 0$. We obtain therefore

$$G = \frac{1}{\beta} \log \left(1 + \beta g \langle \tau \rangle\right) + \left(\frac{1 - g \langle \tau \rangle \varphi_\tau}{1 + \beta g \langle \tau \rangle} - 1 \right) \delta_q + \text{noise} =: \langle G \rangle - \varphi_G \delta_q + \nu_G \ .$$

We obtain then

$$\langle G \rangle = \frac{1}{\beta} \log \left(1 + \beta g \langle \tau \rangle\right) \ .$$

Assuming stationarity, we have that $\langle G \rangle = \log 2$, and therefore

$$g \langle \tau \rangle = \frac{2^\beta - 1}{\beta} \ ,$$

from which we obtain

$$G = \langle G \rangle - \left(\frac{1 - 2^{-\beta}}{\beta} \varphi_\tau + 1 - 2^{-\beta} \right) \delta_q + \text{noise} \ .$$

In the case $\beta = 0$ we obtain $\varphi_G = \varphi_\tau \log 2$. Note that if $\beta = 0$, the factor $\log 2$ is equal to $g \langle \tau \rangle = \langle \alpha \rangle \langle \tau \rangle$ and we recover $\varphi_G = \langle \alpha \rangle \langle \tau \rangle \varphi_\tau$, obtained for exponential growth. For linear growth ($\beta = 1$) we have instead $\varphi_G = (\varphi_\tau + 1)/2$. As expected, a timer ($\varphi_\tau = 0$) corresponds to an adder ($\varphi_G = \lambda = 0.5$) for linear growth. This expresses the well-known fact that, for linear growth, a timer coincides with an adder and is able to perform size correction (Conlon and Raff, 2003), see also section V.A

The exponential growth rate is defined as

$$\alpha = \frac{G}{\tau} \ .$$

By expanding for small δ_q, we obtain an equation giving the fluctuation pattern of α,

$$\alpha = \langle\alpha\rangle(1-\gamma\delta_q)+\text{noise} = \frac{\langle G\rangle - \varphi_G\delta_q + \nu_G}{\langle\tau\rangle(1-\varphi_\tau\delta_q)+\nu_\tau} = \frac{\langle G\rangle}{\langle\tau\rangle}(1+\varphi_\tau\delta_q) - \frac{\varphi_G}{\langle\tau\rangle}\delta_q + \text{subleading terms} \ .$$

By imposing stationarity ($\langle G\rangle = \log 2$) and neglecting subleading terms, we finally obtain

$$\gamma = \frac{\varphi_G}{\langle\alpha\rangle\langle\tau\rangle} - \varphi_\tau = \left(\frac{1-2^{-\beta}}{\beta\langle\alpha\rangle\langle\tau\rangle} - 1\right)\varphi_\tau + \frac{1-2^{-\beta}}{\langle\alpha\rangle\langle\tau\rangle} \ , \tag{9}$$

which is equal to zero if $\beta = 0$ (exponential growth, for which $\langle\alpha\rangle\langle\tau\rangle = \log 2$) and always positive if $\beta > 0$. The limit case $\varphi_\tau = 0$, $\beta = 1$ (timer, linear growth) corresponds to an adder ($\lambda = 1/2$) where all the control is exterted by the growth mode ($\gamma\langle\alpha\rangle\langle\tau\rangle = 1/2$). Note that a positive γ corresponds to homeostatic correction (larger cells grow slower). For intermediate values of β, Eq. (9). gives the expected contribution of the growth mode to size correction, which should be disentangled from size based growth-rate changes at key checkpoints. In order to distinguish such an active modulation of growth rate from passive correction due to sublinear growth (a very subtle question), one needs to access many high-resolution time tracks of growing cells, beyond the currently available statistics.

VI. TESTING THE ADDER BETWEEN TWO REPLICATION INITIATIONS

In both bacteria and daughter cells of budding yeast, where an effective adder for the whole cycle has been reported (Campos et al., 2014; Soifer et al., 2016; Taheri-Araghi et al., 2015), we can distinguish two points of view on the underlying mechanism are currently debated. The first one assumes that the adder is the result of a combination of strong size control in the first period of the cell cycle (B period for *E. coli* and G1 for *S. cerevisiae*) and a weaker near-timer in the second part of the cell cycle (C+D period for *E. coli* and S-G2 for *S. cerevisiae*) (Adiciptaningrum et al., 2015; Delarue et al., 2016; Di Talia et al., 2007; Wallden et al., 2016). An alternative explanation is that a constant volume is added between two replication initiation events, thus overlapping two cell cycles (e.g. the added volume is the sum of volume added during S-G2 of the first cell cycle and the added volume during G1 phase of the subsequent cell cycle) (Amir, 2017; Ho and Amir, 2015; Si et al., 2016; Soifer et al., 2016; Zheng et al., 2016). In daughter cells of budding yeast, the latter model predicts: (i) a positive correlation between volume added during S-G2 (cell generation n) and volume at birth (cell generation $n+1$); (ii) a negative correlation between volume at birth and volume added during G1 phase and finally (iii) an absence of correlation between volume added between two G1/S transitions and volume at birth (Soifer et al., 2016). Additionally (iv) determining whether added volume is less variable from two G1/S transitions or from birth to mitosis would help distinguishing between the two models.

The debate between the two models is unresolved for both budding yeast and bacteria. We sought to test these different correlations with HT29-hgem cells (Figures S3E-G). We could observe a negative correlation between added volume during S-G2 of the mother cell and volume at birth of the daughter (point (i)) and a negative correlation between added volume in G1 and volume at birth (point (ii)). Unfortunately, we lack a sufficient number

of observations of overlapping cell cycles to test predictions (iii) and (iv). To date, our data are not sufficient to point to one of the two pictures for tha case of mammalian cells.

References

Adiciptaningrum, A., Osella, M., Moolman, M. C., Cosentino Lagomarsino, M., and Tans, S. J. (2015). Stochasticity and homeostasis in the E. coli replication and division cycle. *Scientific reports*, 5(November):18261.

Amir, A. (2014). Cell Size Regulation in Bacteria. *Physical Review Letters*, 112(20):208102.

Amir, A. (2017). Is cell size a spandrel? *eLife*, 6:1–8.

Campos, M., Surovtsev, I., Kato, S., Paintdakhi, A., Beltran, B., Ebmeier, S., and Jacobs-Wagner, C. (2014). A Constant Size Extension Drives Bacterial Cell Size Homeostasis. *Cell*, 159(6):1433–1446.

Conlon, I. and Raff, M. (2003). Differences in the way a mammalian cell and yeast cells coordinate cell growth and cell-cycle progression. *Journal of biology*, 2(1):7.

Delarue, M., Weissman, D., and Hallatschek, O. (2016). A simple molecular mechanism explains multiple patterns of cell-size regulation. *bioRxiv*, 1(22):2013–2016.

Di Talia, S., Skotheim, J. M., Bean, J. M., Siggia, E. D., and Cross, F. R. (2007). The effects of molecular noise and size control on variability in the budding yeast cell cycle. *Nature*, 448(7156):947–51.

Dolznig, H., Grebien, F., Sauer, T., Beug, H., and Müllner, E. W. (2004). Evidence for a size-sensing mechanism in animal cells. *Nature cell biology*, 6(9):899–905.

Ginzberg, M. B., Kafri, R., and Kirschner, M. (2015). On being the right (cell) size. *Science*, 348(6236):1245075–1245075.

Godin, M., Delgado, F. F., Son, S., Grover, W. H., Andrea, K., Tzur, A., Jorgensen, P., Payer, K., Grossman, A. D., Marc, W., Manalis, S. R., Bryan, A. K., and Kirschner, M. W. (2010). Using buoyant mass to measure the growth of single cells. *Nature methods*, 7(5):387–90.

Goranov, A. I. and Amon, A. (2010). Growth and division-not a one-way road. *Current Opinion in Cell Biology*, 22(6):795–800.

Grilli, J., Osella, M., Kennard, A. S., and Cosentino Lagomarsino, M. (2017). Relevant parameters in models of cell division control. *Phys. Rev. E*, 95:032411.

Ho, P.-y. and Amir, A. (2015). Simultaneous Regulation of Cell Size and Chromosome Replication in Bacteria. *Frontiers in Microbiology*, 6(July):1–10.

Iyer-Biswas, S., Wright, C. S., Henry, J. T., Lo, K., Burov, S., Lin, Y., Crooks, G. E., Crosson, S., Dinner, A. R., and Scherer, N. F. (2014). Scaling laws governing stochastic growth and division of single bacterial cells. *Proceedings of the National Academy of Sciences*, pages 1403232111–.

Jorgensen, P. and Tyers, M. (2004). How cells coordinate growth and division. *Current biology : CB*, 14(23):R1014–27.

Jun, S. and Taheri-Araghi, S. (2015). Cell-size maintenance: Universal strategy revealed. *Trends in Microbiology*, 23(1):4–6.

Kafri, R., Levy, J., Ginzberg, M. B., Oh, S., Lahav, G., and Kirschner, M. W. (2013). Dynamics extracted from fixed cells reveal feedback linking cell growth to cell cycle. *Nature*, 494(7438):480–483.

Kennard, A. S., Osella, M., Javer, A., Grilli, J., Nghe, P., Tans, S. J., Cicuta, P., and Cosentino Lagomarsino, M. (2016). Individuality and universality in the growth-division laws of single E. Coli cells. *Physical Review E - Statistical, Nonlinear, and Soft Matter Physics*, 93(1):1–18.

Killander, D. and Zetterberg, A. (1965). quantitative cytochemical studies on interphase growth II derivation of synthesis curves from the distribution of DNA, RNA and mass values of individual mouse fibroblasts in vitro. *Experimental Cell Research*, 39:22–32.

Mitchison, J. (2003). Growth During the Cell Cycle. *International Review of Cytology*, 226:165–258.

Osella, M., Nugent, E., and Cosentino Lagomarsino, M. (2014). Concerted control of Escherichia coli cell division. *Proceedings of the National Academy of Sciences of the United States of America*, 111(9):3431–5.

Osella, M., Tans, S. J., and Cosentino Lagomarsino, M. (2017). Step by Step, Cell by Cell: Quantification of the Bacterial Cell Cycle. *Trends in Microbiology*, xx:1–7.

Park, K., Millet, L. J., Kim, N., Li, H., Jin, X., Popescu, G., Aluru, N. R., Hsia, K. J., and Bashir, R. (2010). Measurement of adherent cell mass and growth. *Proceedings of the National Academy of Sciences of the United States of America*, 107(48):20691–6.

Si, F., Li, D., Cox, S. E., Sauls, J. T., Azizi, O., Schwartz, A. B., and Erickstad, M. J. (2016). Deconstructing cell size control into physiological modules in Escherichia coli. *bioRxiv*, (1):1–23.

Soifer, I., Robert, L., and Amir, A. (2016). Single-cell analysis of growth in budding yeast and bacteria reveals a common size regulation strategy. *Current Biology*, 26(3):356–361.

Son, S., Tzur, A., Weng, Y., Jorgensen, P., Kim, J., Kirschner, M. W., and Manalis, S. R. (2012). Direct observation of mammalian cell growth and size regulation. *Nature Methods*, 9(9):910–912.

Sung, Y., Tzur, A., Oh, S., Choi, W., Li, V., Dasari, R. R., Yaqoob, Z., and Kirschner, M. W. (2013). Size homeostasis in adherent cells studied by synthetic phase microscopy. *Proceedings of the National Academy of Sciences of the United States of America*, 110(41):16687–92.

Taheri-Araghi, S., Bradde, S., Sauls, J., Hill, N., Levin, P., Paulsson, J., Vergassola, M., and Jun, S. (2015). Cell-Size Control and Homeostasis in Bacteria. *Current Biology*, 25(3):385–391.

Turner, J. J., Ewald, J. C., and Skotheim, J. M. (2012). Cell size control in yeast. *Current Biology*, 22(9).

Tzur, A., Kafri, R., Lebleu, V. S., Lahav, G., and Kirschner, M. W. (2009). Cell growth and size homeostasis in proliferating animal cells. *Science (New York, N.Y.)*, 325(5937):167–71.

Wallden, M., Fange, D., Gregorsson Lundius, E., Baltekin, Ö., and Elf, J. (2016). The synchronization of replication and division cycles in individual E. coli cells (in press). *Cell*, pages 729–739.

Wang, P., Robert, L., Pelletier, J., Dang, W. L., Taddei, F., Wright, A., and Jun, S. (2010). Robust growth of escherichia coli. *Current Biology*, 20(12):1099–1103.

Zheng, H., Ho, P.-Y., Jiang, M., Tang, B., Liu, W., Li, D., Yu, X., Kleckner, N. E., Amir, A., and Liu, C. (2016). Interrogating the Escherichia coli cell cycle by cell dimension perturbations. *Proceedings of the National Academy of Sciences*, page 201617932.

SUPPLEMENTARY FIGURE 1 (part1)

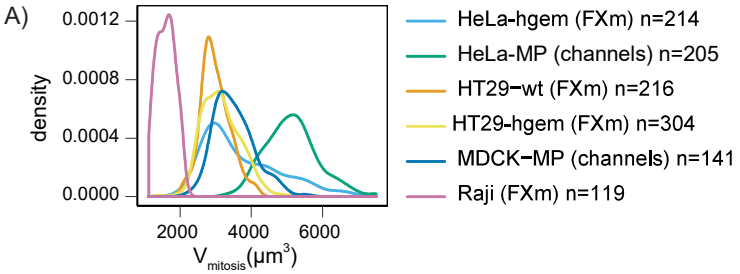

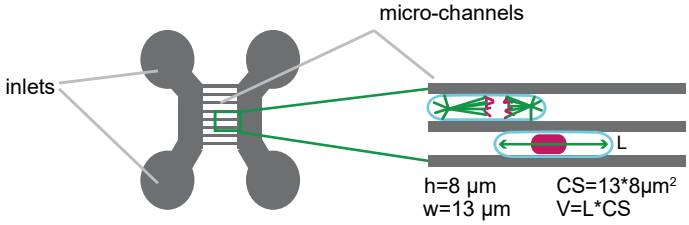

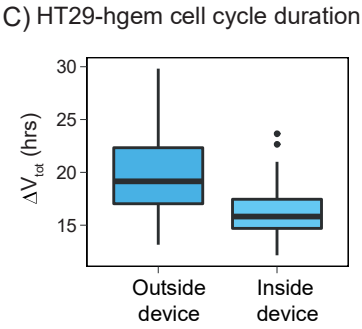

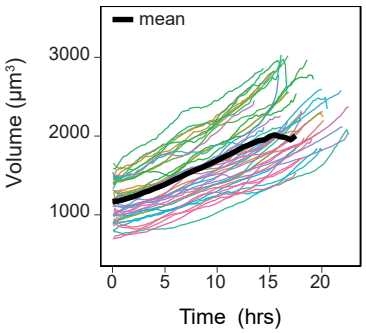

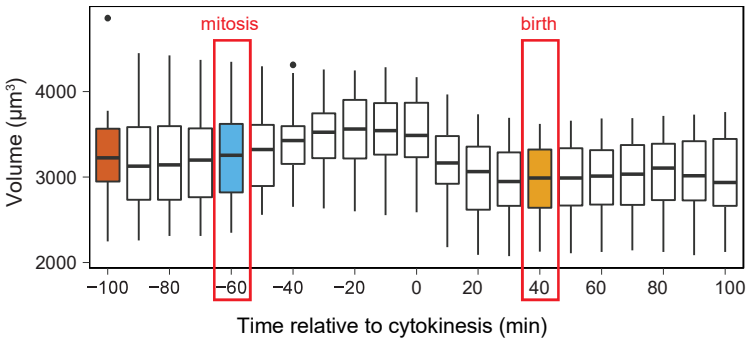

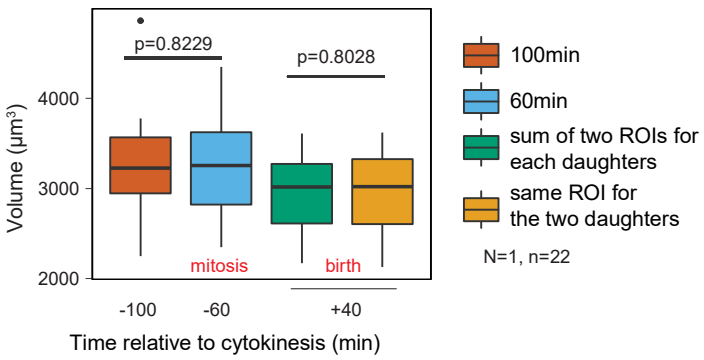

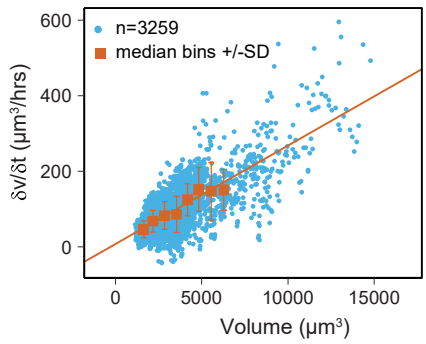

SUPPLEMENTARY FIGURE 1 (part2)

H) Control of growth quality for each experiment

HT29 (FXm)

number of cells per experiment:

- n = 75
- n = 105
- n = 100

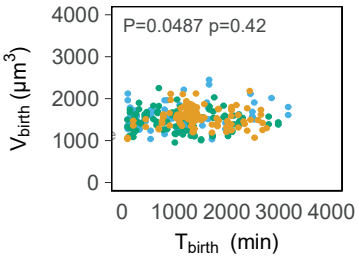

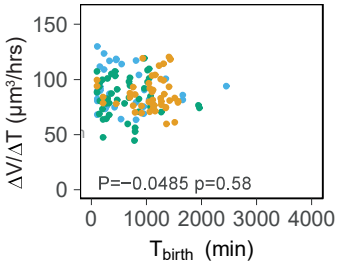

HT29-hgem (FXm)

number of cells per experiment:

- n = 31
- n = 20
- n = 41
- n = 49

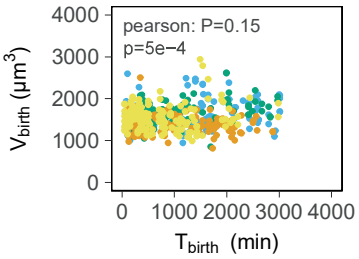

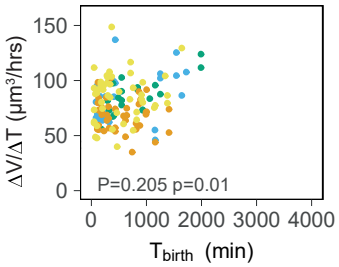

HeLa-hgem (FXm)

number of cells per experiment:

- n = 97
- n = 61

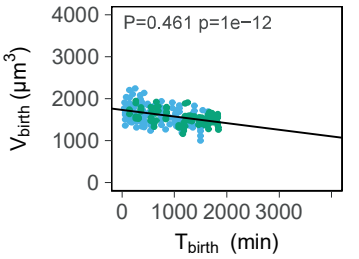

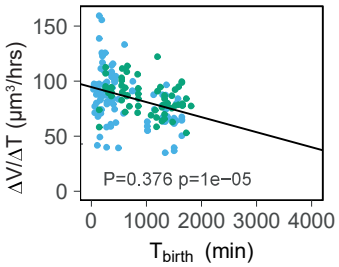

Raji (FXm)

number of cells per experiment:

- n = 50
- n = 58

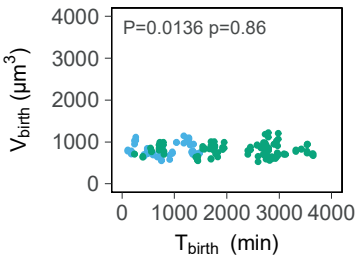

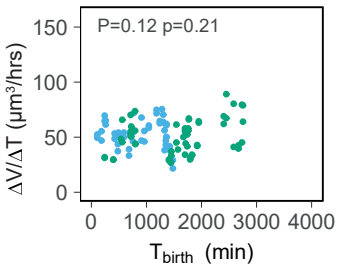

HeLa-MyrPalm (channels)

number of cells per experiment:

- n = 38
- n = 59
- n = 40

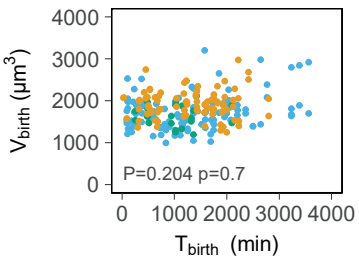

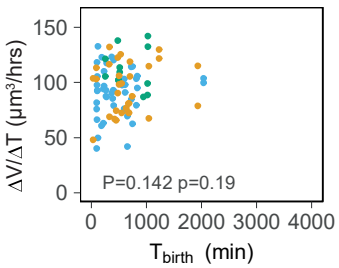

MDCK-MyrPalm (channels)

number of cells per experiment:

- n = 44
- n = 12
- n = 31

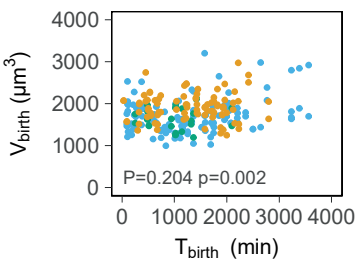

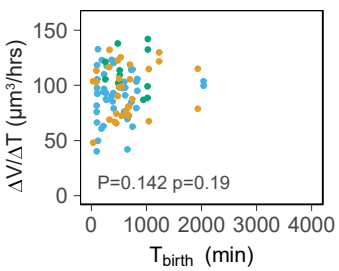

SUPPLEMENTARY FIGURE 2 (part 1)

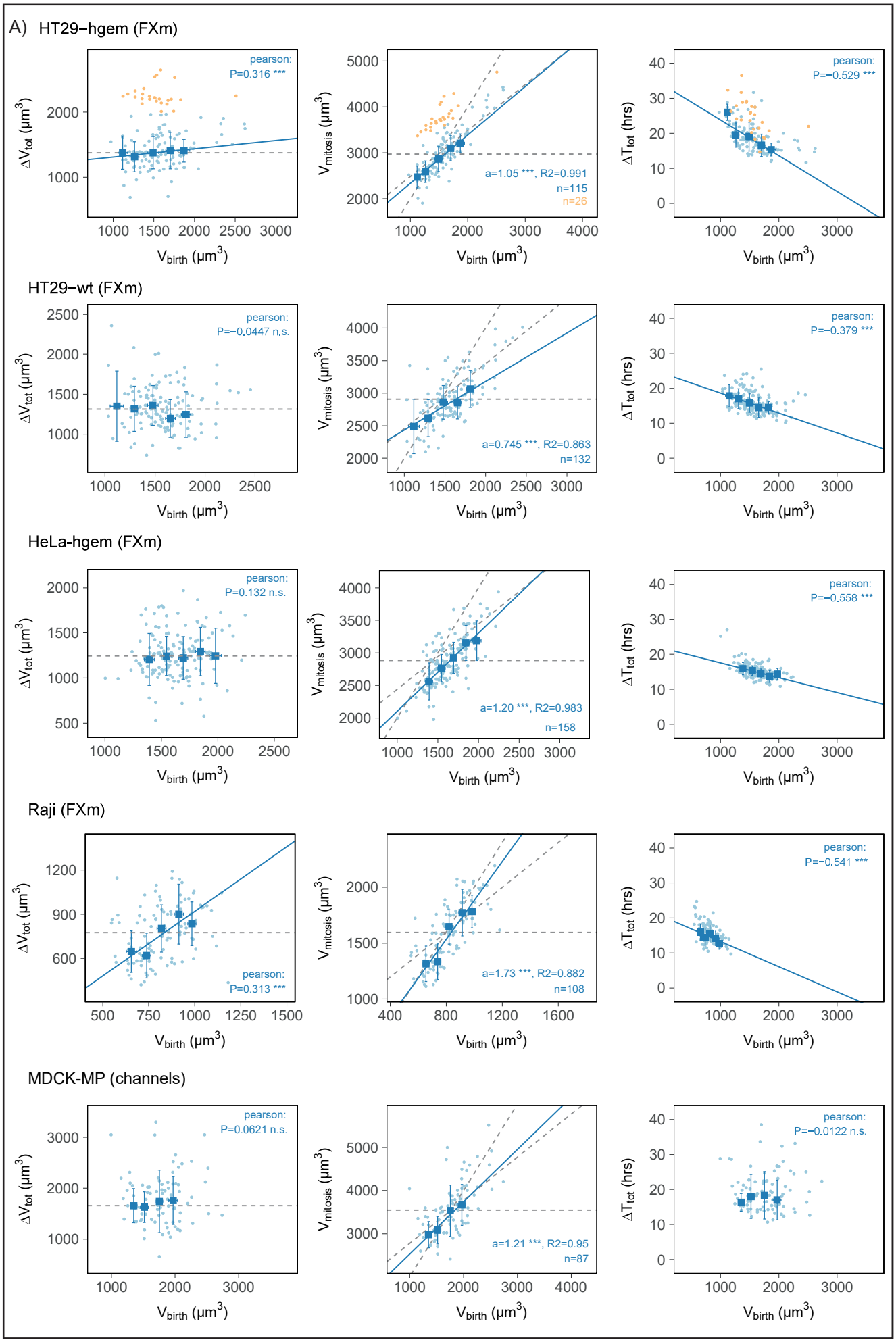

SUPPLEMENTARY FIGURE 2 (part 2)

A) continued

HeLa-MP (channels)

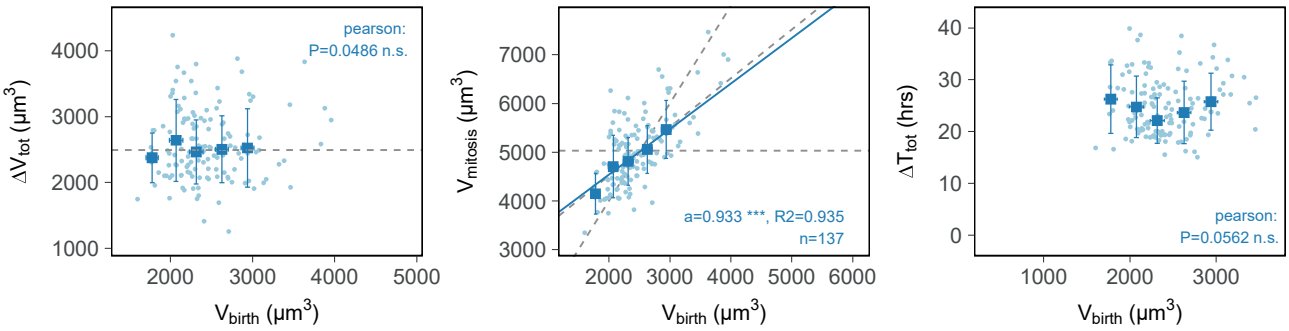

B)

unconfined:HeLa-hgem (FXm)

confined: HeLa-MP (channels)

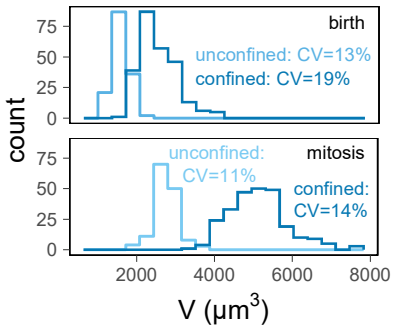

SUPPLEMENTARY FIGURE 3 (part 1)

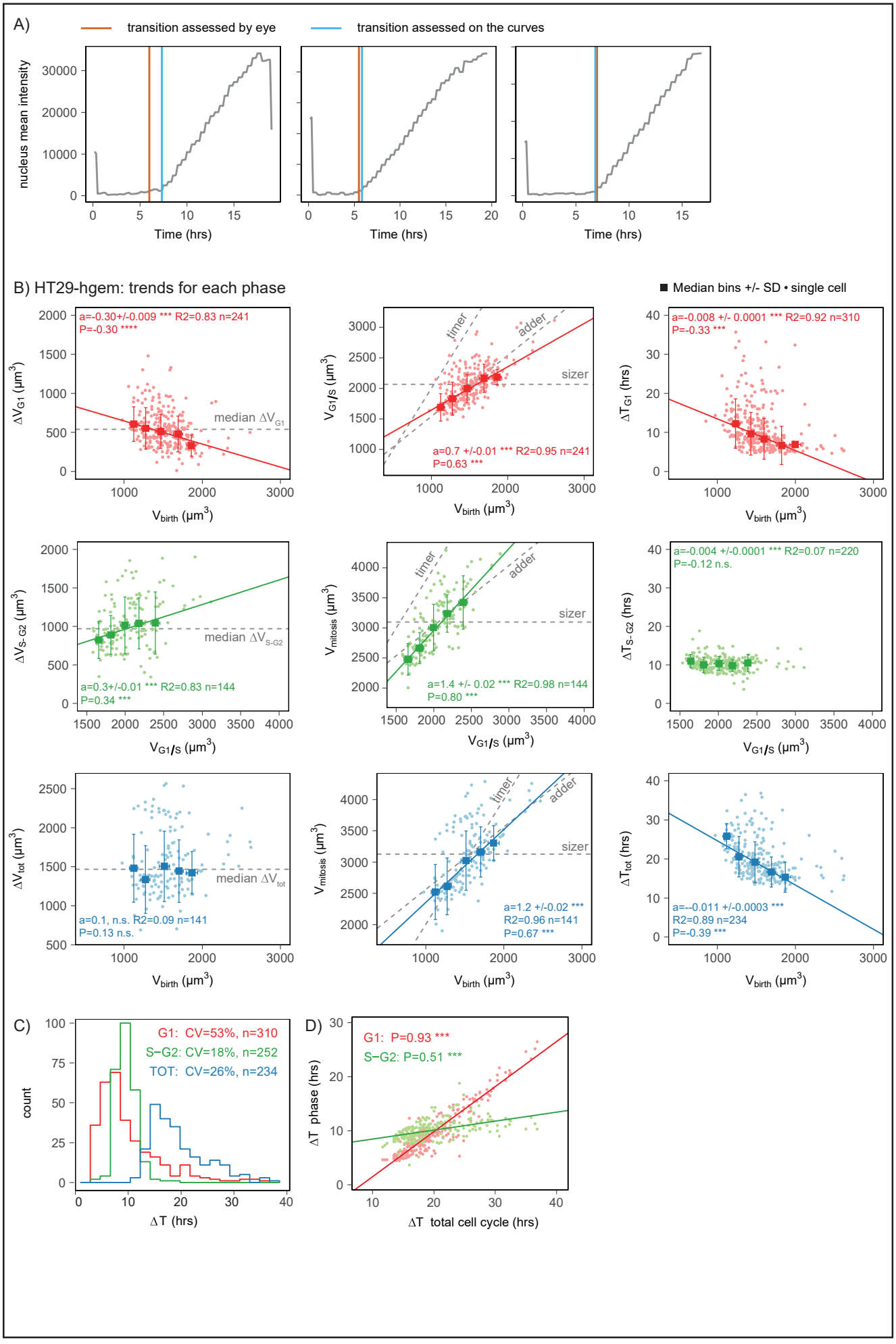

SUPPLEMENTARY FIGURE 3 (part 2)

SUPPLEMENTARY FIGURE 4

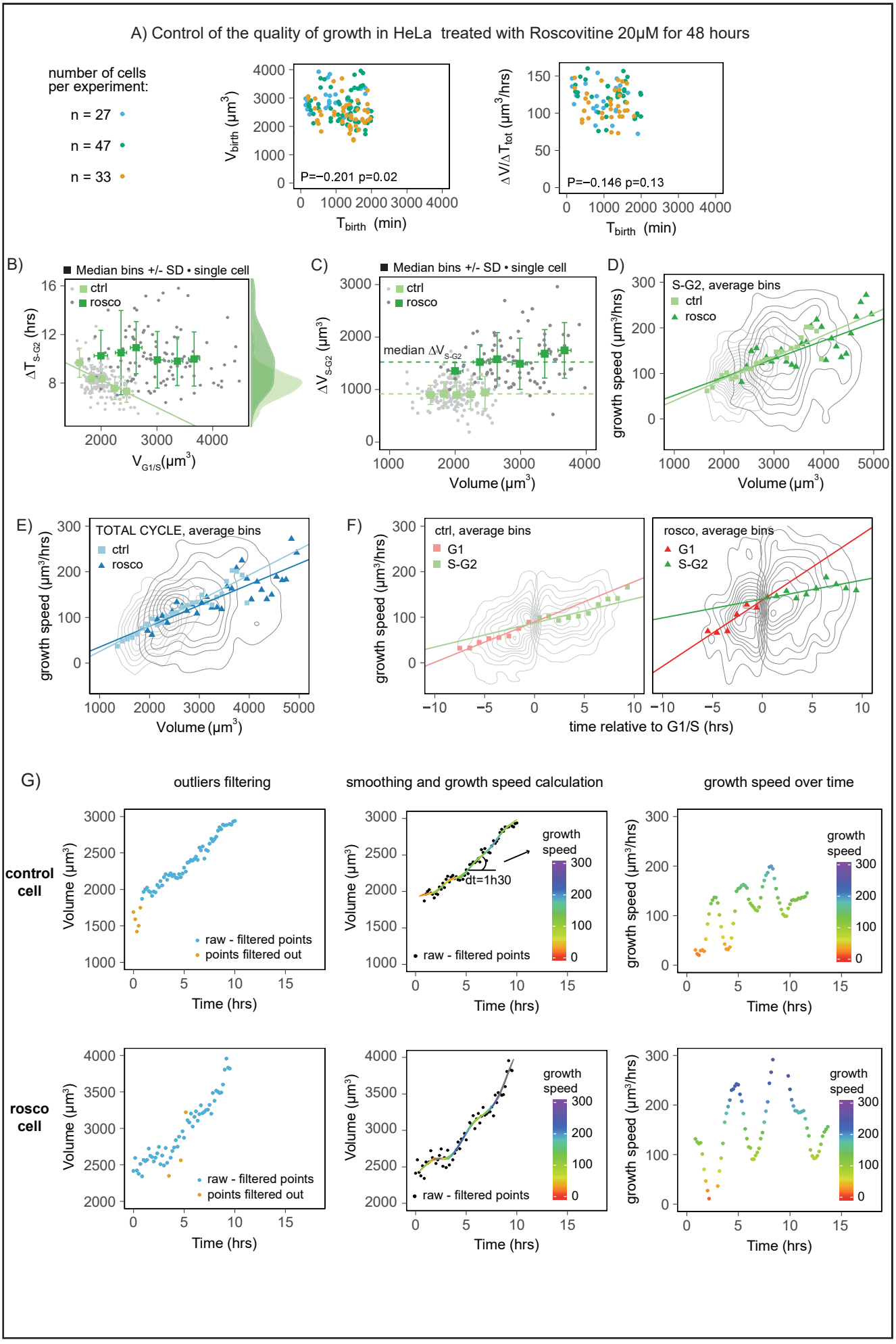

SUPPLEMENTARY FIGURE 4 part 2

H) Example of single volume curves - HeLa control cells

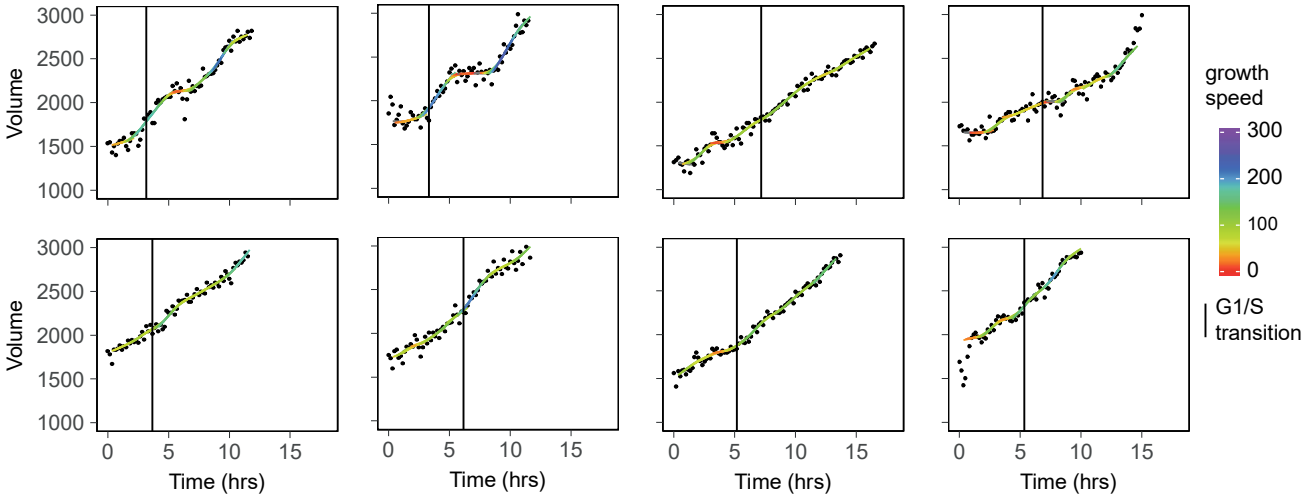

I) Example of single volume curves - HeLa rosco cells

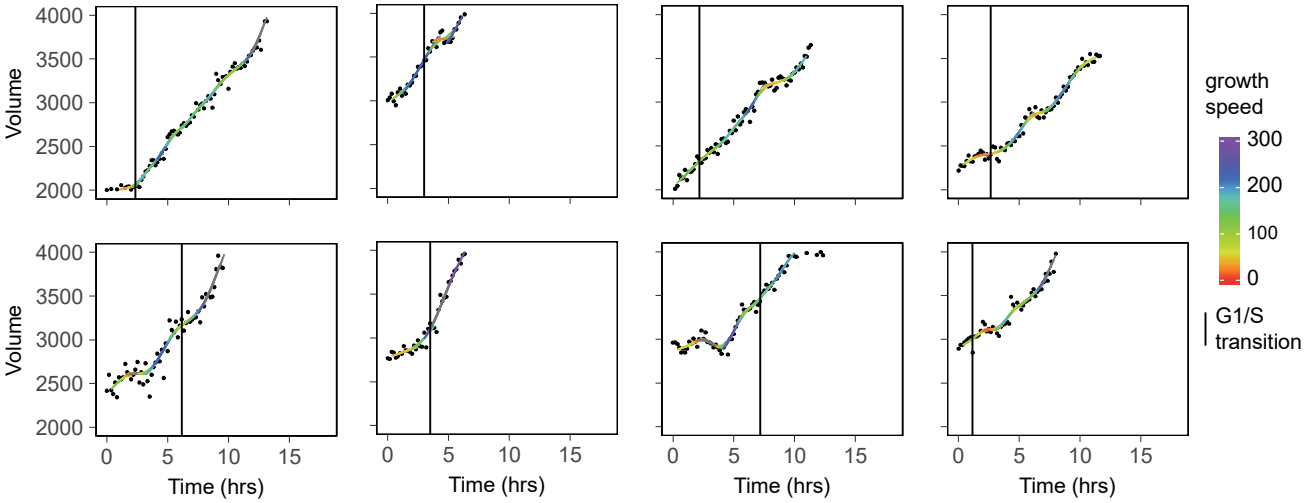

SUPPLEMENTARY FIGURE 5 (part 1)

	Example eukaryote: HT29-WT	Example Bacteria: E.Coli_MRR_LB
A) size-growth plot: $\alpha\tau_{Vi} = <\alpha\tau> - \lambda\,(\log(V_i) - <\log(V_i)>)$	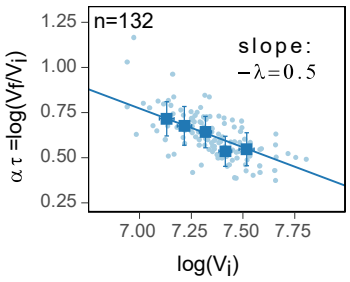	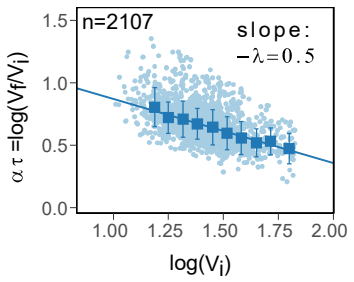
B) time vs. size $\tau_{Vi} = <\tau> - \theta\,(\log(V_i) - <\log(V_i)>)$	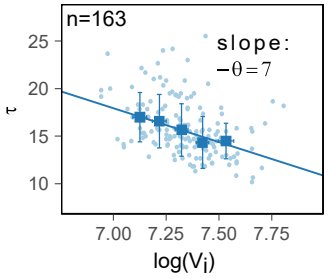	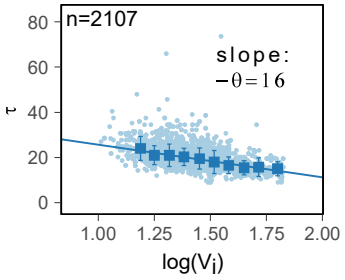
C) growth rate vs. size $\alpha_{Vi} = <\alpha> - \gamma\,(\log(V_i) - <\log(V_i)>)$	$\gamma = (\lambda - \theta<G>) / <G><\tau>$	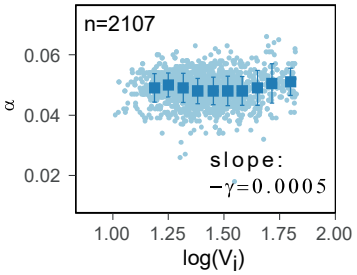

D) Validation of the method of trends estimation using the covariance in bacteria and yeast data sets

Bacteria and yeasts

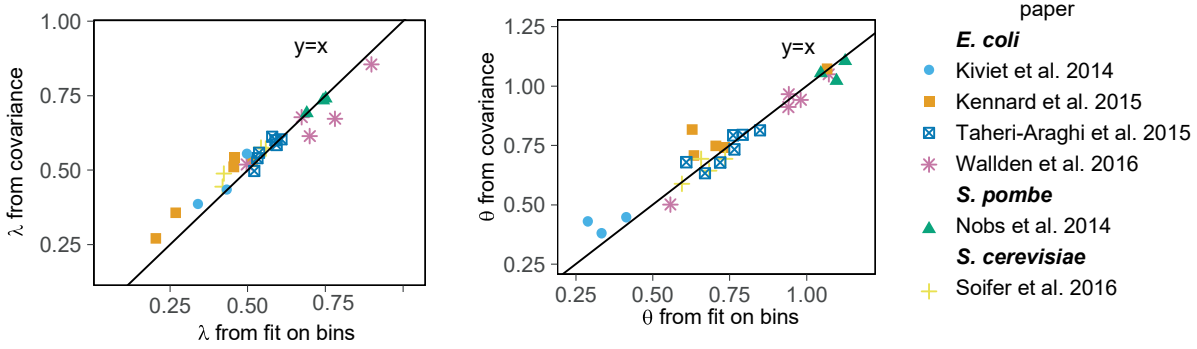

Animal cells

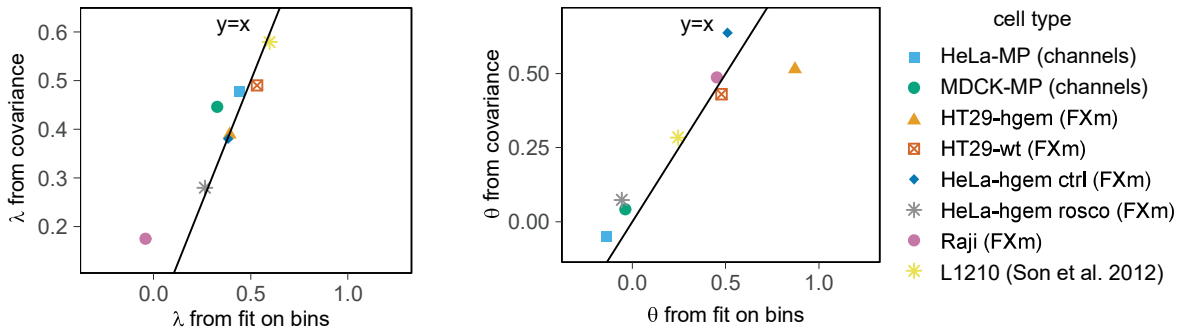

SUPPLEMENTARY FIGURE 5 (part 2)

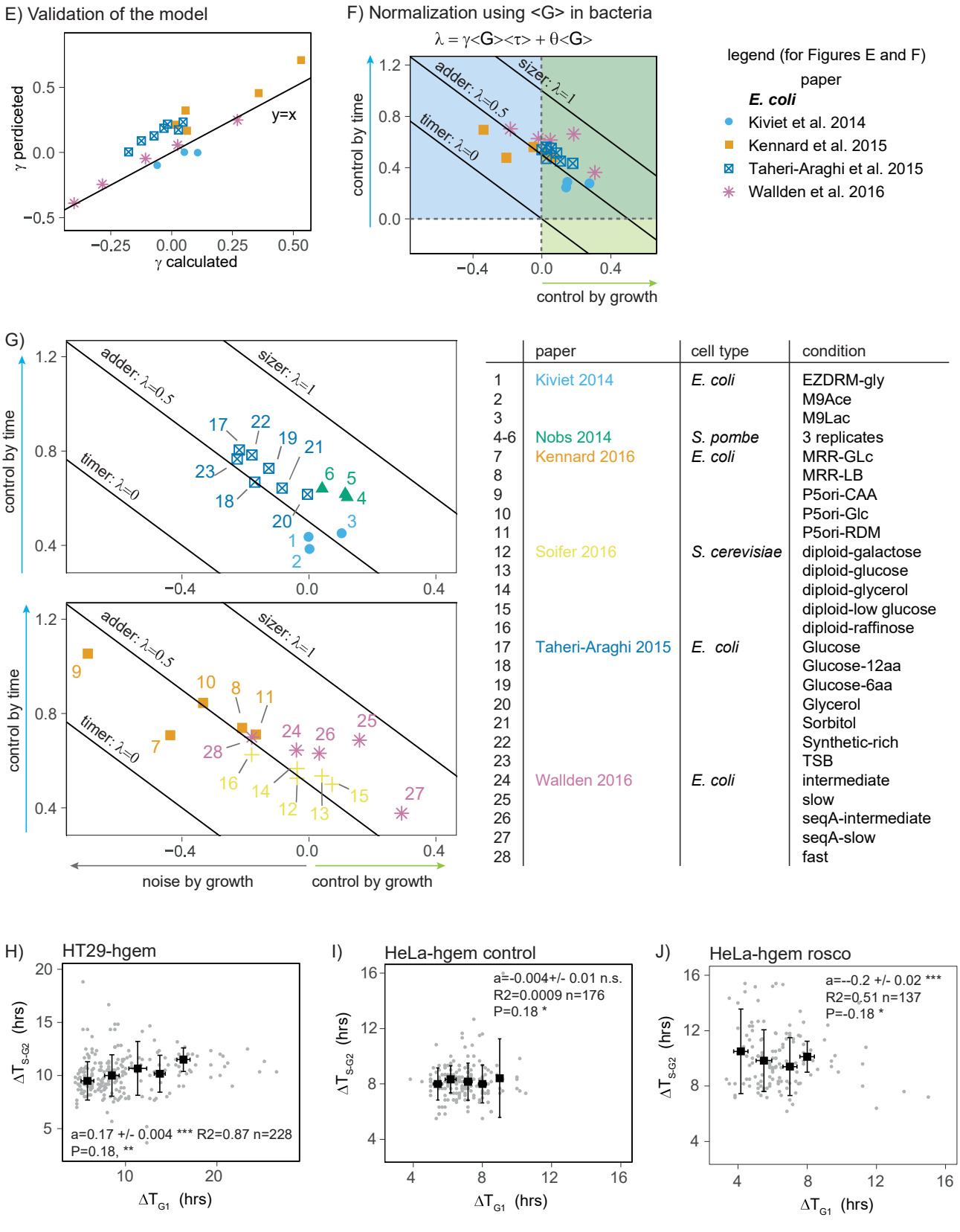

	paper	cell type	condition
1	Kiviet 2014	*E. coli*	EZDRM-gly
2			M9Ace
3			M9Lac
4-6	Nobs 2014	*S. pombe*	3 replicates
7	Kennard 2016	*E. coli*	MRR-GLc
8			MRR-LB
9			P5ori-CAA
10			P5ori-Glc
11			P5ori-RDM
12	Soifer 2016	*S. cerevisiae*	diploid-galactose
13			diploid-glucose
14			diploid-glycerol
15			diploid-low glucose
16			diploid-raffinose
17	Taheri-Araghi 2015	*E. coli*	Glucose
18			Glucose-12aa
19			Glucose-6aa
20			Glycerol
21			Sorbitol
22			Synthetic-rich
23			TSB
24	Wallden 2016	*E. coli*	intermediate
25			slow
26			seqA-intermediate
27			seqA-slow
28			fast